Targeting TLR4 during vaccination boosts MAdCAM-1^{+} lymphoid stromal cell activation and promotes the aged germinal center response

Alice E Denton[1,2,*], James Dooley[1,3], Isabella Cinti[2], Alyssa Silva-Cayetano[1], Sigrid Fra-Bido[1], Silvia Innocentin[1], Danika L Hill[1,4], Edward J Carr[1,5,6], Andrew NJ McKenzie[7], Adrian Liston[1,3] and Michelle A Linterman[1]

[1] Immunology Programme, Babraham Institute, Cambridge UK.

[2] Department of Immunology and Inflammation, Imperial College London, London UK.

[3] Adaptive Immunology Laboratory, VIB and University of Leuven, Leuven Belgium.

[4] Department of Immunology and Pathology, Central Clinical School, Monash University and Alfred Hospital, Melbourne, Victoria, Australia.

[5] Department of Medicine, University of Cambridge, Cambridge UK.

[6] The Francis Crick Institute, London UK.

[7] Medical Research Council, Laboratory of Molecular Biology, Cambridge, UK.

* Correspondence: a.denton@imperial.ac.uk

Abstract

The failure to generate enduring humoral immunity after vaccination is a hallmark of advancing age. This can be attributed to a reduction in the germinal center (GC) response, which generates long-lived antibody-secreting cells that protect against (re)infection. Despite intensive investigation, the primary cellular defect underlying impaired GCs in aging has not been identified. Here, we used heterochronic parabiosis to demonstrate that GC formation was dictated by the age of the lymph node (LN) microenvironment, rather than the age of the immune cells. Lymphoid stromal cells are a key determinant of the LN microenvironment and are also an essential component underpinning GC structure and function. Using mouse models of immunization, we demonstrated that Mucosal adressin cell adhesion molecule (MAdCAM)-1-expressing lymphoid stromal cells were among the first cells to respond to NP-KLH+Alum immunization, proliferating and upregulating cell surface proteins such as podoplanin and cell adhesion molecules. This response was essentially abrogated in aged mice. By targeting TLR4 using novel adjuvants, we improved the MAdCAM-1$^+$ stromal cell response to immunization. Importantly, this correlated with improved GC responses – in both younger adult and aged mice – suggesting a link between stromal cell responses to immunization and GC initiation. We also found, using bone marrow chimeras, that MAdCAM-1$^+$ stromal cells could respond directly to TLR4 ligands. Thus the age-associated defect in GC and stromal cell responses to immunization are a surmountable barrier to efficacious vaccination in older people.

Once Sentence Summary

Targeting TLR4 with GLA-SE adjuvant boosts lymphoid stromal cell and GC responses to protein immunization in aged mice.

Main text

Introduction

While the extension of human life expectancy is a great achievement of the modern era, it creates a challenge for science: to facilitate healthy aging. Older individuals are at higher risk of infection partly due to decreased functionality of the immune system (*1*). Vaccination is an effective preventative strategy for limiting the negative health consequences from infection, however older people often do not generate long-lasting protective immunity after vaccination (*2-5*). Understanding why older individuals do not respond well to vaccines is key to developing the next generation of immunization strategies that will be effective in older people.

The generation of durable humoral immunity requires the production of memory B cells and plasma cells that secrete high affinity class-switched antibodies (*6*). Long-lived memory B and plasma cells are the ultimate output of the germinal center (GC), a specialized immune response that typically forms in secondary lymphoid organs (*7*). The GC reaction requires the concerted efforts of many different cell types that must be coordinated in time and space. B cells, T follicular helper (Tfh) cells, dendritic cells and macrophages are brought together by a network of specialized stromal cells that provide migratory cues that direct cells to, and within, the GC (*8*). The GC response is diminished with advancing age (reviewed in (*9*)) with the size and number of GCs, the generation of memory B cells and plasma cells, and the production of antigen-specific antibody all reduced in older people. B cell age does not largely alter their capacity to participate in a GC (*10*), while T cell responses, in contrast, are impaired in older individuals. Notably, the magnitude of the Tfh cell response is reduced in mice and humans (*11-13*), and their ability to support GC formation (*14*) and B cell selection (*10*) is impaired by age. Despite these findings, rescuing Tfh cell formation in aged mice is not sufficient to rescue the GC response (*12*), suggesting other mechanisms contribute to poor GC formation in aging.

The LN microenvironment is largely dictated by the stromal cell network, which offers a physical scaffold for immune cell migration, as well as supplying migration, adhesion and survival cues that influence immune cell localization and behavior (*15*). The depletion of lymphoid stromal cells abrogates adaptive immune responses (*16, 17*), and the responses of lymphoid stromal cells to immune challenge are important for the development of adaptive immunity (*18-22*). In aging, lymphoid tissue architecture is disrupted, and defects in stromal cell function, such as altered chemokine expression, are linked with loss of appropriate immune cell segregation and impaired T cell survival (*23-27*), and this is associated with diminished adaptive immune responses (*28, 29*). In the context of humoral immunity, the GC forms after vaccination and its two zones are supported by distinct stromal cell subsets. The light zone is supported by follicular dendritic cells (FDCs), which are essential for the GC (*30*) as they produce the chemokine CXCL13 and act as a depot for antigen (*31*), while the dark zone is populated by CXCL12-abundant reticular cells whose functions are poorly defined outside of their role as a migratory nexus (*32-34*). Marginal reticular cells (MRCs), have also been suggested to play a role in GC formation as they may contribute to antigen transport (*35, 36*) and can act as a progenitor for *de novo* FDC differentiation (*37*), although they are otherwise poorly defined. In aged mice, lymphoid stromal cells have delayed expansion in response to infection (*29*), but their response to immunization and whether age-associated lymphoid stromal cell changes contribute to the defective GC reaction has not been fully explored.

Here, we used heterochronic parabiosis, in which younger adult and aged mice share a circulatory system, to demonstrate that the age of the LN microenvironment was a key determinant of poor GC formation in aging. This correlated with impaired expansion of the stromal cell network that underpins the B cell follicle. This effect was most striking in MAdCAM-1$^+$ lymphoid stromal cells, and our data showed that the initiation of the stromal

cell response to vaccination could not be rejuvenated by exposure to young immune cells. MAdCAM-1$^+$ lymphoid stromal cells underwent transcriptional and cellular changes in response to immunization and this response was almost completely absent in aged mice. Finally, this roadblock in aging immunity could be improved by targeting the TLR4 pathway during immunization, and this correlated with improved GC responses. In sum, we identified the transcriptional and cellular responses of MAdCAM-1$^+$ lymphoid stromal cells to immunization and demonstrated that these are defective in aging. Furthermore, we showed that these age-dependent defects in stromal cell and GC responses could be rejuvenated by targeted adjuvant selection.

Results

Age-associated defects in GC formation are driven by the LN microenvironment

To confirm that GC responses are impaired in older animals in our model, we subcutaneously immunized adult (8-12 week old) and aged (>95 week old) Balb/c mice with NP-KLH+Alum and tracked the GC response over 21-days based on expression of the typical GC markers ki67 and Bcl-6 (Fig 1A), gated on B cells (gating strategy in Fig S1A). Total LN cellularity (Fig S1B) and the absolute number of B cells (Fig S1C) were both diminished, and the GC B cell response was reduced in both proportion (Fig 1B) and absolute number (Fig 1C). These studies were consistent between mice of different genetic backgrounds: C57BL/6 mice show a similar reduction in LN cellularity (Fig S1D) and number of B cells (Fig S1E), as well as the proportion (Fig 1D, E) and absolute number (Fig 1F) of GC B cells seven days after immunization with NP-KLH+Alum. The diminished GC response led to a reduced GC output after NP-KLH+Alum immunization in aging, where the number of both low (Fig 1G) and high (Fig 1H) affinity antibody-secreting cells (ASCs) in the bone marrow were reduced and there was a reduction in affinity maturation of these cells in aged C57BL/6 mice (Fig 1I). This was coupled to a reduction in antigen-specific IgG levels detected in serum for both low and high affinity antibodies (Fig 1J).

While immune cell-intrinsic age-associated defects have been associated with the reduced GC response in age, a number of studies suggest that the aged LN microenvironment is also associated with diminished immune responses (*25, 38, 39*). To definitively determine whether the age of immune cells or the age of the LN microenvironment was the primary driver of poor initiation of GC responses, we established a model of heterochronic parabiosis. Parabiosis is a procedure through which the circulatory system of animals is surgically conjoined, generating a system in which blood-derived cells are shared across individual mice and non-migratory cells remain that of the original host (*40*). Thus, this system allowed us to interrogate the role(s) of immune cells and the LN microenvironment in the aged GC.

We generated three groups of parabiotic pairs using congenically distinct C57BL/6 mice: an adult isochronic group, where adult mice were parabiosed with mice of the same age (6-12 weeks; red); an aged isochronic group, where aged mice were parabiosed with aged mice (>92 weeks; blue); and a heterochronic group, where younger adult (6-12 weeks) mice were parabiosed with aged (>92 weeks) mice (Fig 1K). Mice were cohoused in pairs for two weeks prior to surgery to allow for social conditioning and rested for three weeks after surgery to allow revascularization and establishment of parabiosis. Mice were immunized with NP-KLH+Alum on outer flanks (contralateral to the surgical site) and seven days after immunization we determined the GC response (Fig 1L). Parabiosis was determined by CD45.1:CD45.2 chimerism of B cells in the blood of parabiotic pairs (Fig 1M) and confirmed in the non-GC B cell ($B220^{+}Bcl6^{-}ki67^{-}$) compartment of reactive LNs (Fig 1N). We found no significant difference in the establishment of blood parabiosis between the groups, although the aged isochronic group showed more variability, while some preference for self-derived B cells was observed in adult:adult parabionts.

To determine whether the age of the microenvironment contributes to the initiation of the GC, we measured the size of the total GC response in adult:adult isochronic, aged:aged isochronic and adult:aged heterochronic pairs by determining the proportion of $ki67^{+}Bcl\text{-}6^{+}$ GC B cells amongst $B220^{+}$ B cells seven days after immunization (Fig 1O). Consistent with the observed age-associated defect in GC formation (Fig 1A-F), the aged isochronic pairs had fewer GC B cells than younger adult isochronic pairs (Fig 1P). In heterochronic pairs, the magnitude of the GC reaction was dictated by the age of the host: the GC response was significantly reduced in aged animals, even though the B cell pool derived from both adult and aged mice (Fig 1P). This suggested that the age of the microenvironment dictated the size of the GC response. To further investigate this, we exploited the fact that the immune cells are congenically marked ($CD45.1^{+}$ or $CD45.2^{+}$), allowing us to determine whether B cell-intrinsic

aging influenced their capacity to participate in the GC using heterochronic parabionts. We classified B cells based on the age of the donor from which they were derived and determined their contribution to the GC response in both adult and aged LNs. We found that B cells from adult mice were impaired in their capacity to generate GC B cells in an aged LN (Fig 1Q). In agreement with this, B cells from aged mice participated in the GC response comparably to those from younger adult mice if they were in a younger LN (Fig 1Q). Thus, the age of the LN microenvironment, rather than that of the B cells, dictated the capacity to generate GC responses in an aged setting.

Age impairs the expansion of LN stromal cells in response to immunization

Lymphoid stromal cells are a key determinant of the LN microenvironment and are a diverse population of cells whose functions are still being clearly defined (*41*). Lymphoid stromal cells are essential for GC formation and maintenance (*8*), and are non-migratory, and therefore could contribute to the age-dependent defect in GC formation caused by the microenvironment (Fig 1). We investigated how two populations of lymphoid stromal cells respond to immunization, FDCs and MAdCAM-1$^+$ lymphoid stromal cells. FDCs are essential to the GC response (*30*). MAdCAM-1$^+$ lymphoid stromal cells, in naïve lymph nodes, are typically found at the subcapsular sinus (SCS):follicle border, and this includes marginal reticular cells (MRCs) , which are key contributors to the GC stromal cell network following immunization (*37*). To investigate how the responses of these cells to immunization were affected by age, we subcutaneously immunized adult (8-12 week old) and aged (>95 week old) Balb/c mice with NP-KLH+Alum and determined the expansion of MAdCAM-1$^+$ lymphoid stromal cells and FDCs over 21-days. FDCs were identified as CD21/35$^+$ and MAdCAM-1$^+$ lymphoid stromal cells were identified as MAdCAM-1$^+$ and lack of CD21/35 (Fig 2A), both within the CD45$^-$CD31$^-$Pdpn$^+$ population (gating strategy in Fig S2A). We observed a trend towards a reduction in MAdCAM-1$^+$ lymphoid stromal cells as a proportion of CD45$^-$CD31$^-$Pdpn$^+$ stromal cells seven days after immunization with NP-KLH+Alum (Fig

2B) and a 6-fold reduction in the absolute number of MAdCAM-1$^+$ lymphoid stromal cells at the same timepoint (Fig 2C) in aged mice. This early defect in MAdCAM-1$^+$ lymphoid stromal cell number was associated with a reduction in the proportion and number of FDCs in aged mice (Fig 2D, E), compared to younger adult Balb/c mice. To determine whether these results were consistent between strains of mice, we immunized C57BL/6 mice with NP-KLH+Alum and determined MAdCAM-1$^+$ lymphoid stromal cell and FDC responses seven days after immunization, based on MAdCAM-1 and CD21/35 expression (Fig 2F). We observed a significant reduction in both the proportion and absolute number of MAdCAM-1$^+$ lymphoid stromal cells (Fig 2G, H) and FDCs (Fig 2I, J) in aged C57BL/6 mice. This demonstrated that age impaired the expansion of stromal cells that were associated with the GC.

To establish whether the impaired stromal cell response in aged mice was cell-intrinsic or could be altered by the presence of lymphocytes from an animal of a different age, we used heterochronic parabiosis, performed as in (Fig 1K, L). We measured the expansion of MAdCAM-1$^+$ lymphoid stromal cells and FDCs as a proportion of CD45$^-$CD31$^-$Pdpn$^+$ stromal cells (Fig 2K) in adult:adult isochronic, aged:aged isochronic and adult:aged heterochronic mice. In isochronic pairs, the expansion of MAdCAM-1$^+$ lymphoid stromal cells (Fig 2L) and FDCs (Fig 2M) was significantly diminished in aged mice, compared to younger adult mice, consistent with our findings in non-parabiosed aged mice (Fig 2A-J). In heterochronic parabionts, we observed that the expansion of MAdCAM-1$^+$ lymphoid stromal cells was significantly diminished in the aged mouse compared to its adult partner (Fig 2L). A similar trend was observed for the expansion of FDCs in heterochronic parabionts, where FDCs expanded poorly in aged mice (Fig 2M).

To determine whether the poor expansion of MAdCAM-1$^+$ lymphoid stromal cells and FDCs was specific to immunization, we also measured the frequency and absolute number of

different lymphoid stromal cell subsets in resting LNs obtained from younger adult and aged C57BL/6 mice. While the total LN cellularity was reduced in aged mice compared to younger adults (Fig 2N), the number of fibroblastic reticular cells (FRCs), defined as MAdCAM-1$^-$ CD21/35$^-$Pdpn$^+$CD31$^-$CD45$^-$, was not altered by age (Fig 2O). This suggested that age did not alter the absolute number of lymphoid stromal cells in the lymph node, as FRCs are the bulk of this population. We did, however, find that both the absolute number of MAdCAM-1$^+$ lymphoid stromal cells (Fig 2P) and FDCs (Fig 2Q) were reduced in LNs from older C57BL/6 mice. This was reflected in the reduced frequency of MAdCAM-1$^+$ lymphoid stromal cells and FDCs in aged C57BL/6 mouse LNs (Fig 2R-T). The reduced number and frequency of MAdCAM-1$^+$ lymphoid stromal cells and FDCs observed by flow cytometry in resting aged LNs was also reflected in staining for these cells by microscopy (Fig 2U). Together these data indicated that age impacts the maintenance of MAdCAM-1$^+$ lymphoid stromal cells and FDCs, but not FRCs, and that their ability to respond to immunization is diminished by advanced age. The impaired expansion of lymphoid stromal cells in aged mice could not be rescued by exposure to leukocytes derived from younger adult mice seven days after immunization, suggesting a cell-intrinsic defect in their response to immune challenge.

MAdCAM-1$^+$ lymphoid stromal cells dynamically respond to immunization

The capacity of lymphoid stromal cells to respond to infection and immunization, and its impact on immune responses, is a rapidly developing field. To date, most studies have investigated the bulk population of Pdpn$^+$ FRCs, which contains several cell types which may respond differently to stimulation. To further investigate the global response of FDCs and MAdCAM-1$^+$ lymphoid stromal cells to immunization, we sort-purified FDCs and MAdCAM-1$^+$ lymphoid stromal cells from adult C57BL/6 mouse LNs before and two days after immunization with NP-KLH+Alum and subjected them to bulk RNA sequencing. We performed transcriptome analysis two days after immunization so we could understand how lymphoid stromal cells respond to the immunization, rather than how lymphoid stromal cells

was were impacted by a poor adaptive immune response – a potential confounder in aging. MAdCAM-1$^+$ lymphoid stromal cells and FDCs were purified to 80% and >95% purity, respectively (Fig S2B). We also found that the distribution of MAdCAM-1 expression was similar in non-draining (nd)LNs and draining (d)LNs obtained two days after NP-KLH+Alum immunization (Fig S2C), being largely restricted to the SCS:follicle border, in line with expression chiefly by MRCs. The successful isolation of MAdCAM-1$^+$ lymphoid stromal cells and FDCs was confirmed by the expression of genes typically associated with these cells (*41*), and lack of immune and endothelial cell-related markers such as *Cd3e*, *Cd19*, *Itga7* or *Pecam1* (Figure S3A). Principal Component Analysis (PCA), performed on the 1000 most variable genes, demonstrated that FDCs and MAdCAM-1$^+$ lymphoid stromal cells comprised distinct cell types, which was maintained two days after immunization (Fig 3A). The vast majority of clustering was driven by PC1, separating FDCs from MAdCAM-1$^+$ lymphoid stromal cells, giving little separation of immunized and naïve cells within each subset. Thus, we further interrogated the effect of immunization by re-running analyses separately for each cell type. We found little separation of FDCs based on immunization status or age (Fig S3B, C) indicating that this cell type did not undergo significant transcriptional change within two days of immunization. In contrast, we saw distinct separation of immunized and unimmunized MAdCAM-1$^+$ lymphoid stromal cells (Fig 3B), where 2881 genes were differentially expressed (Fig 3C), which suggested widespread transcriptional remodeling. Genes involved in glycolysis (*Gapdh*) and protein synthesis (*Rpl7a*) as well as chemokines (*Cxcl9*) and cell surface proteins such as *Ly6a* were among the top differentially expressed genes (Fig S3D). This indicated that immunization affects multiple aspects of the MAdCAM-1$^+$ lymphoid stromal cell transcriptome.

To better understand the transcriptional changes that occur to MAdCAM-1$^+$ lymphoid stromal cells after immunization, we performed gene set enrichment analysis (GSEA). We found enrichment of pathways associated with angiogenesis, notch signaling and DNA damage in MAdCAM-1$^+$ lymphoid stromal cells isolated from unimmunized mice, whilst

genesets associated with immune responses (Ifna response, Ifng response, inflammatory response), initiation of proliferation (E2F targets, Myc targets, Mtorc1 signaling) and the unfolded protein response were enriched in MAdCAM-1$^+$ lymphoid stromal cells isolated from immunized mice (Fig 3D). These findings suggested that MAdCAM-1$^+$ lymphoid stromal cells proliferated after immunization and were sensitive the inflammatory environment induced by immunization.

To confirm these observations, we immunized adult (8–12week-old) C57BL/6 mice with NP-KLH+Alum and determined the MAdCAM-1$^+$ lymphoid stromal cell response four days later. While our data showed that, two days after immunization, the distribution of MAdCAM-1 expression was similar to that observed in naïve LNs (Fig S2C), by day four MAdCAM-1 was also expressed by T-zone stromal cells, albeit weaker than that observed on MRCs at the SCS (Fig S2D), in line with previous findings during viral infection (*42*). We confirmed these results by flow cytometry: MAdCAM-1$^+$ lymphoid stromal cells expanded early after immunization, representing an increased proportion of CD45$^-$CD31$^-$CD21/35$^-$ Pdpn$^+$ stromal cells (Fig 3E, F) and a greater absolute number in dLNs compared to ndLNs (Fig 3G). To further understand the activation phenotype of MAdCAM-1$^+$ lymphoid stromal cells, we investigated the upregulation of cell surface markers previously shown to be upregulated by lymphoid stromal cells (*22, 43, 44*): Pdpn, ICAM-1, VCAM-1 and CD44, as well as MAdCAM-1 as the defining marker for these cells. We found that MAdCAM-1$^+$ lymphoid stromal cells upregulated all these markers four days after immunization (Fig 3H-L), although this was not necessarily reflected at the transcriptional level in RNAseq data obtained two days after immunization (Figure S3H). These findings suggested that MAdCAM-1$^+$ lymphoid stromal cells acquired an activated phenotype in response to immunization in our model.

Consistent with a proliferative transcriptional signature in MAdCAM-1$^+$ lymphoid stromal cells two days after immunization, a higher proportion of MAdCAM-1$^+$ lymphoid stromal cells expressed ki67 in dLNs compared to ndLNs when analyzed four days after

immunization with NP-KLH+Alum (Fig 3M, N). To confirm that SCS-adjacent MRCs proliferate in response to vaccination, we used confocal microscopy to identify ki67-expressing RANKL$^+$ cells located between the SCS and the B cell follicle (Fig 3O), consistent with the described localization of MAdCAM-1$^+$ MRCs (*34*). Together these data demonstrated that MAdCAM-1$^+$ lymphoid stromal cells, including SCS-adjacent MRCs, underwent a range of transcriptional, phenotypic, and functional alterations in response to NP-KLH+Alum immunization.

Aging impairs the MAdCAM-1$^+$ lymphoid stromal cell response to immunization

Given the impaired expansion of MAdCAM-1$^+$ lymphoid stromal cells in aging (Fig 2) and the myriad of changes that occurred in MAdCAM-1$^+$ lymphoid stromal cells after immunization (Fig 3), we next determined how aging affected the MAdCAM-1$^+$ lymphoid stromal cell response to immunization. We performed bulk RNA sequencing of sort-purified MAdCAM-1$^+$ lymphoid stromal cells isolated from aged C57BL/6 mouse LNs before and two days after immunization with NP-KLH+Alum, as was conducted for younger adult mice (Fig 3A-D). MAdCAM-1$^+$ lymphoid stromal cell identity was confirmed by the expression of genes typically associated with this cell type (*41*), and lack of FDC, immune and endothelial cell-related genes (Figure S3A). PCA performed on the 1000 most variable genes demonstrated that, unlike that observed in younger adult MAdCAM-1$^+$ lymphoid stromal cells (Fig 3B), aged MAdCAM-1$^+$ lymphoid stromal cells did not clearly separate based on immunization status (Fig 4A). The poor response to immunization by aged MAdCAM-1$^+$ lymphoid stromal cells was confirmed by DESeq2 analysis, where 289 genes were differentially expressed following immunization (Fig 4B). While some genes upregulated after immunization in aged MAdCAM-1$^+$ lymphoid stromal cells (Fig S3E) were shared with the gene expression changes observed after immunization in MAdCAM-1$^+$ lymphoid stromal cells derived from younger adult mice (Fig S3D), such as *Rpl7* and *Gapdh* (Fig S3E), the global transcriptome changes observed in MAdCAM-1$^+$ lymphoid stromal cells from younger

adult mice were largely not conserved in aged mice. 2811 genes were differentially expressed in younger adult MAdCAM-1$^+$ lymphoid stromal cells after immunization compared to just 289 genes in aged MAdCAM-1$^+$ lymphoid stromal cells, with 141 of these genes shared (Fig 4C). This suggested that the immunization-induced transcriptional changes in MAdCAM-1$^+$ lymphoid stromal cells were severely blunted in aged mice. Indeed, PCA conducted on MAdCAM-1$^+$ lymphoid stromal cell samples from both adult and aged mice analyzed together demonstrated that MAdCAM-1$^+$ lymphoid stromal cells isolated from immunized younger adult mice clustered separately from the other three groups (Fig 4D). MAdCAM-1$^+$ lymphoid stromal cells isolated from immunized aged mice did not cluster distinctly, indicative of a failed response to immunization in aged mice.

To further understand how age affects the MAdCAM-1$^+$ lymphoid stromal cell transcriptome, we investigated how gene expression differed between younger adult and aged MAdCAM-1$^+$ lymphoid stromal cells obtained from naïve mice. We saw 280 differentially expressed genes between aged and adult mice (Fig 4E), indicating that age does not significantly impair the transcriptome of MAdCAM-1$^+$ lymphoid stromal cells in the resting state. This was in stark contrast to that observed between the transcriptomes of aged and adult immunized MAdCAM-1$^+$ lymphoid stromal cells, where 2828 genes were differentially expressed (Fig 4F). We found that some genes, for example MHC class II molecules (*H2-Eb1*, *H2-DMa*, *H2-Aa*), were among the genes with the highest fold change between adult and aged MRCs in both resting and immunized MAdCAM-1$^+$ lymphoid stromal cells (Fig S3F, G). To better understand how aging affected the global transcriptome of MAdCAM-1$^+$ lymphoid stromal cells, we performed GSEA on the RNA sequencing data from younger adult and aged MAdCAM-1$^+$ lymphoid stromal cells isolated two days after immunization using the Hallmark gene sets. We found several gene sets that were differentially enriched between immunized adult and aged MAdCAM-1$^+$ lymphoid stromal cells (Fig 4G). Some of these sets were also altered after immunization in younger adult MAdCAM-1$^+$ lymphoid stromal cells

(Fig 3D): Myc targets, Mtorc1 signaling and the Ifna response. This suggested that the response of MAdCAM-1$^+$ lymphoid stromal cells to immunization was compromised in aging, and this impairment occurred early after immunization. To confirm these findings, we investigated the early responses of MAdCAM-1$^+$ lymphoid stromal cells to immunization in aged mice. We found that, four days after NP-KLH+Alum immunization, the expansion of MAdCAM-1$^+$ lymphoid stromal cells was diminished in aged mice (Fig 4H), both as a proportion of CD45$^-$CD31$^-$CD21/35$^-$Pdpn$^+$ stromal cells (Fig 4I) and in absolute number (Fig 4J). This correlated with a reduced proportion of proliferating MAdCAM-1$^+$ lymphoid stromal cells in aged mice (Fig 4K, L). We also found that the upregulation of Pdpn on MAdCAM-1$^+$ lymphoid stromal cells was impaired in aged mice (Fig 4M, N), indicative of poor MAdCAM-1$^+$ lymphoid stromal cell activation.

To understand how the transcriptional remodeling of MAdCAM-1$^+$ lymphoid stromal cells contributed to their activation and the generation of GC responses, we elected to investigate genes or gene families that were differentially expressed in younger adult, but not aged, MAdCAM-1$^+$ lymphoid stromal cells after immunization with NP-KLH+Alum. IL-33 was one such gene, where *Il33* was upregulated after immunization in MAdCAM-1$^+$ lymphoid stromal cells younger adult mice, but not in MAdCAM-1$^+$ lymphoid stromal cells isolated from aged mice (Fig S4A). We confirmed our RNA sequencing results using *Il33*$^{cit/cit}$ reporter mice, in which the fluorescent protein, Citrine, has been knocked in to the *Il33* locus (*45*). We found that IL-33 expression, as measured by Citrine Mean Fluorescence Intensity (MFI), was upregulated in MAdCAM-1$^+$ lymphoid stromal cells isolated from the dLN four days after immunization with NP-KLH+Alum (Fig S4B) and remained elevated at day seven (Fig S4C), compared to that observed in MAdCAM-1$^+$ lymphoid stromal cells isolated from ndLNs. The absence of IL-33 did not, however, alter the activation of MAdCAM-1$^+$ lymphoid stromal cells (Fig S4D-H) or the formation of GCs in this immunization model (Fig S4I-L). Thus, the

failure to upregulate IL-33 in response to vaccination did not contribute to the poor MAdCAM-1$^+$ lymphoid stromal cell and GC responses observed in older mice.

The induction of type I interferon (IFN) in response to immunization is impaired in aging (*46*). Enhancing type I IFN production in aged mice promotes the activation and differentiation of Tfh cells that support the GC response (*12*), suggesting that dysregulation of type I IFN signaling could be linked to the poor stromal cell responses observed in aged mice. Our RNAseq analysis of MAdCAM-1$^+$ lymphoid stromal cells demonstrated that the Ifna pathway was enriched after immunization with NP-KLH+Alum in younger adult mice (Fig 3D), but not in aged mice (Fig 4G). Further probing of our RNAseq data showed that expression of type I IFN-responsive mRNAs was increased after immunization in younger adult mice, but not in aged mice (Fig S5A). To determine whether lack of type I IFN signaling impacted on the ability of MAdCAM-1$^+$ lymphoid stromal cells to respond to immunization, we administered NP-KLH+Alum to *Ifnar*$^{-/-}$ and C57BL/6 (control) mice and determined the MAdCAM-1$^+$ lymphoid stromal cell response four days later. We found that lack of type I IFN signaling did not alter the total LN cellularity (Fig S5B), and that the MAdCAM-1$^+$ lymphoid stromal cell response was largely intact, measured in proportion, absolute number, proliferation and upregulation of Pdpn expression (Fig S5C-H). Thus, while poor type I IFN induction in response to immunization is a hallmark of the vaccine response in aged individuals, this response was not essential for MAdCAM-1$^+$ lymphoid stromal cell responses to immunization.

TLR4 promotes MAdCAM-1$^+$ lymphoid stromal cell responses

Our data demonstrated that Alum was a poor stimulator of MAdCAM-1$^+$ lymphoid stromal cell responses in aged mice (Fig 4). The exact mode of action of Alum remains controversial (*47*), with the NALP3 inflammasome the most strongly indicated mechanistic pathway (*48*). Newer, effective adjuvants include molecules designed to stimulate specific pattern

recognition receptors (*49*), thus we elected to investigate which pathogen-detecting receptors MAdCAM-1$^+$ lymphoid stromal cells may express in order to identify an effective adjuvant through which these cells could be directly targeted. We probed our transcriptomic data for the expression of pattern recognition receptors and found that MAdCAM-1$^+$ lymphoid stromal cells expressed *Tlr1, Tlr2*, *Tlr3*, and *Tlr4*, as well as the major signaling components associated with *Tlr4*, including *Cd14* and *Myd88* (Fig 5A). Other TLRs were below the cutoff for gene expression in our dataset, except *Tlr6* which had very low mRNA expression levels. *Tlr4*, *Myd88*, and *Cd14* were highly expressed by MAdCAM-1$^+$ lymphoid stromal cells compared to FDCs (Fig 5A), thus we elected to further investigate its expression. We confirmed that MAdCAM-1$^+$ lymphoid stromal cells expressed cell surface TLR4 and CD14 by flow cytometry (Fig 5B, C), and this suggested that MAdCAM-1$^+$ lymphoid stromal cells may directly respond to TLR4 agonists.

To determine whether TLR4 stimulation could induce MAdCAM-1$^+$ lymphoid stromal cells responses *in vivo*, we administered PBS, Alum, or 5μg LPS emulsified in Alum to adult C57BL/6 mice and determined the MRC response four days later. The administration of Alum alone was not sufficient to induce a MAdCAM-1$^+$ lymphoid stromal cell response, however the addition of LPS to Alum induced MAdCAM-1$^+$ lymphoid stromal cell activation, including expansion of MAdCAM-1$^+$ lymphoid stromal cells (Fig 5D, E), proliferation (Fig 5F) and upregulation of Pdpn, VCAM-1, ICAM-1, and CD44 (Fig 5G-J), but no significant difference in the level of MAdCAM-1 expression (Fig 5K). The fact that administration of Alum alone did not induce an MAdCAM-1$^+$ lymphoid stromal cell response was surprising, but consistent with experiments where we directly compared the MAdCAM-1$^+$ lymphoid stromal cells response to immunization with Alum with or without the protein antigen, NP-KLH (Fig S6A-D).

To determine whether we could boost MAdCAM-1$^+$ lymphoid stromal cell responses to vaccination with adjuvants targeting TLR4, we used GLA-SE (glucopyranosyl lipid-A in a stable oil-in-water emulsion), a TLR4-stimulating adjuvant (*50*) that promotes adaptive immunity in a number of different vaccine settings in humans and mice (*51-56*). We subcutaneously immunized adult C57BL/6 mice with NP-KLH emulsified in GLA-SE or the control Alum-like adjuvant, Alhydrogel (AL007), and determined the MAdCAM-1$^+$ lymphoid stromal cell response four days later. We found that GLA-SE significantly increased the proportion (Fig 5L, M) and absolute number (Fig 5N) of MAdCAM-1$^+$ lymphoid stromal cells, as well as the proportion of MAdCAM-1$^+$ lymphoid stromal cells that were proliferating (Fig 5O), compared to AL007. Moreover, compared to AL007, GLA-SE also increased the expression of Pdpn, VCAM-1, ICAM-1, and CD44 (Fig 5P-S), but not MAdCAM-1 (Fig 5T), mimicking the phenotype of MAdCAM-1$^+$ lymphoid stromal cells in the LPS+Alum immunization (Fig 5D-K). The enhanced MAdCAM-1$^+$ lymphoid stromal cell response induced by GLA-SE correlated with an improved immune response at the same time point, where the total LN cellularity, number of B cells and the proportion and absolute number of GC B cells were increased in GLA-SE compared to AL007 immunization (Fig S6E-H). The improved GC response to GLA-SE was also observed 21 days after immunization, where the absolute number of GC B cells, although not their frequency, was increased in GLA-SE immunization (Fig 5U-W), as were total LN cellularity (Fig S6I) and the absolute number of B cells (Fig S6J). The increased GC response also resulted in a significant increase in the number of high (Fig 5X) and low (Fig 5Y) affinity ASCs in bone marrow, although no change in the impaired affinity maturation was observed between adjuvants (Fig 5Z). Consistent with this, the generation of high (Fig S6K) and low (Fig S6L) affinity serum antibody responses was enhanced by GLA-SE, up to 16-fold, 21 days after immunization, with no significant difference in affinity maturation observed (Fig S6M).

To demonstrate that TLR4 signaling was responsible for inducing the enhanced responsiveness of MAdCAM-1$^+$ lymphoid stromal cells to GLA-SE, we subcutaneously immunized adult *Tlr4*$^{-/-}$ and C57BL/6 control mice with NP-KLH emulsified in AL007 or GLA-SE on contralateral flanks and determined the MAdCAM-1$^+$ lymphoid stromal cell response four days later. We found that the ability of GLA-SE to promote the expansion of MAdCAM-1$^+$ lymphoid stromal cells in the dLN was abrogated in *Tlr4*$^{-/-}$ mice, as measured by the proportion of MAdCAM-1$^+$ cells (Fig 6A, B), absolute number (Fig 6C) and the proportion of MAdCAM-1$^+$ lymphoid stromal cells that were proliferating (Fig 6D). We also found that the enhanced activation of MAdCAM-1$^+$ lymphoid stromal cells by GLA-SE, as measured by expression of Pdpn, VCAM-1 and CD44, was also abrogated in the absence of *Tlr4* (Fig 6E-G).

These data demonstrated that TLR4 signaling was important for the ability of GLA-SE to promote the MAdCAM-1$^+$ lymphoid stromal cell response *in vivo*. To determine whether stromal cell-expressed TLR4 was involved in this enhanced response, we generated bone marrow chimeras where stromal cells lacked expression of TLR4, but immune cells were TLR4-sufficient. We reconstituted lethally irradiated C57BL/6 or *Tlr4*$^{-/-}$ mice (both CD45.2$^+$) with CD45.1$^+$ C57BL/6.SJL mouse bone marrow (Fig S6N), and eight weeks after reconstitution, chimeras were immunized on opposing flanks with NP-KLH emulsified in AL007 or GLA-SE. Four days later, we determined the MAdCAM-1$^+$ lymphoid stromal cell response (Fig S6N). The proportion (Fig S6O) and number (Fig S6P) of MAdCAM-1$^+$ lymphoid stromal cells were not increased in GLA-SE immunization compared to AL007, suggesting that irradiation may have impacted the responsiveness of MAdCAM-1$^+$ lymphoid stromal cells to TLR4-targeted immunization. We did, however, find that all other measures of MAdCAM-1$^+$ lymphoid stromal cell activation, i.e. proliferation and cell surface phenotype, were enhanced by GLA-SE immunization in both control and *Tlr4*$^{-/-}$ hosts (Fig S6Q-U). This suggested that TLR4 expression by MAdCAM-1$^+$ lymphoid stromal cells was

not essential to their activation, and that signaling through immune cell-expressed TLR4 was a key driver of LN stromal cell responsiveness.

To formally test whether direct sensing of TLR4 by MAdCAM-1$^+$ lymphoid stromal cells could influence their response to immunization, we generated bone marrow chimeras in which TLR4 expression was restricted to radioresistant cells by reconstituting lethally irradiated CD45.1$^+$ C57BL/6.SJL mice with C57BL/6 or *Tlr4*$^{-/-}$ bone marrow (both CD45.2$^+$) (Fig 6H). Eight weeks after reconstitution, chimeras were immunized on opposing flanks with NP-KLH emulsified in AL007 or GLA-SE and the MAdCAM-1$^+$ lymphoid stromal cell response was determined four days later (Fig 6H). As above, we found that neither the proportion (Fig 6I) nor number (Fig 6J) of MAdCAM-1$^+$ lymphoid stromal cells was increased in GLA-SE immunization compared to AL007. When we investigated other measures of MAdCAM-1$^+$ lymphoid stromal cell activation, we found that while proliferation was dependent on TLR4 expression in immune cells (Fig 6K), both Pdpn (Fig 6L) and VCAM-1 (Fig 6M) expression were increased in GLA-SE immunization in the absence of TLR4 signaling on immune cells, although ICAM-1 (Fig 6N) and CD44 (Fig 6O) expression were not altered. This suggested that sensing of TLR4 by MAdCAM-1$^+$ lymphoid stromal cells, in the absence of immune-mediated TLR4 signaling, can directly impact their activation status.

To understand the impact on TLR4 sensing by lymphoid stromal cells on the generation of the GC response, we measured multiple features of the GC response in each set of chimeras. We found that TLR4 expression by immune cells was essential for the increased LN cellularity (Fig 6P), total B cell number (Fig 6Q) and the enhanced frequency (Fig 6R) and absolute number (Fig 6S) of GC B cells observed four days after NP-KLH+GLA-SE immunization, and that the lack of TLR4 expression by lymphoid stromal cells did not alter these features of

the GC response (Fig S6V-Y). Taken together these data suggested that direct sensing of TLR4 by MAdCAM-1$^+$ lymphoid stromal cells influenced their phenotype *in vivo*.

A TLR4-containing adjuvant boosts the MAdCAM-1$^+$ lymphoid stromal cell response in aged mice

Our data thus far demonstrate that the proliferation and activation of MAdCAM-1$^+$ lymphoid stromal cells was impaired in aged mice, and that administration of TLR4-stimulating ligands could boost MAdCAM-1$^+$ lymphoid stromal cell responsiveness. Our RNA sequencing data also showed that age did not impact on the expression of TLR ligands by MAdCAM-1$^+$ lymphoid stromal cells, as *Tlr4*, *Myd88* and *Cd14* expression were maintained (Fig 7A). This led us to hypothesize that TLR4-mediated stimulation may offer a mechanism through which the impaired MAdCAM-1$^+$ lymphoid stromal cell response in ageing could be improved. To investigate this, we subcutaneously immunized adult and aged C57BL/6 mice on opposing flanks with NP-KLH emulsified in GLA-SE or AL007 (Fig 7B) and determined the MAdCAM-1$^+$ lymphoid stromal cell response four days later. We found that GLA-SE increased the frequency of MAdCAM-1$^+$ lymphoid stromal cells in adult and aged mice (Fig 7C, D); this correlated with an increase in the absolute number of MAdCAM-1$^+$ lymphoid stromal cells in adult mice, and a trend towards an increase in the number of MAdCAM-1$^+$ lymphoid stromal cells in aged mice (Fig 7E). In both adult and aged mice, NP-KLH+GLA-SE increased the proportion of MAdCAM-1$^+$ lymphoid stromal cells that were proliferating (Fig 7F) as well as the level of Pdpn, VCAM-1, ICAM-1 and CD44 (Fig 7G-J), but not MAdCAM-1 expression (Fig 7K), compared to that observed in NP-KLH+AL007 immunized LNs. We also confirmed the enhanced expansion of MAdCAM-1$^+$ lymphoid stromal cells in NP-KLH+GLA-SE immunization by immunofluorescent imaging (Fig S7A, B).

The enhanced MAdCAM-1$^+$ lymphoid stromal cell response in aged C57BL/6 mice four days after NP-KLH+GLA-SE immunization correlated with improved GC responses at the same

timepoint, as evidenced by the increased LN cellularity (Fig S7C), number of B cells (Fig S7D) and the frequency (Fig S7E) and absolute number (Fig S7F) of GC B cells in NP-KLH+GLA-SE immunization, compared to NP-KLH+AL007, in aged mice. To determine whether the enhanced early GC responses in GLA-SE-immunized aged mice was maintained in fully developed GCs, we immunized younger adult and aged C57BL/6 mice with NP-KLH emulsified in AL007 or GLA-SE and determined the GC response and its output 21 days later. NP-KLH+GLA-SE immunization increased the frequency of GC B cells in aged mice (Fig 7L, M), and the absolute number of GC B cells increased but did not reach statistical significance between NP-KLH+AL007 and NP-KLH+GLA-SE in aged mice (Fig 7N). We also measured the generation of low and high affinity ASCs in the bone marrow (Fig 7O-Q) and serum antibodies (Fig 7R-T) 21 days after immunization of younger adult and aged C57BL/6 mice and found that while NP-KLH+GLA-SE immunization increased these parameters in younger adult mice (compared to NP-KLH+AL007), this was not significant in aged mice - perhaps due to the high level of inter-individual variation in ageing, or the inability of NP-KLH+GLA-SE immunization to increase LN cellularity or the total number of B cells in aged mice (Fig S7G, H). Taken together our data demonstrated that TLR4-adjuvanted vaccines increased MAdCAM-1$^+$ lymphoid stromal cell responsiveness aged mice and accelerated the initiation of the GC, but that this did not fully rescue their peak GC or bone marrow plasma cell responses.

Discussion

The diminishing immune responses of aged people is linked to increased risk of infection. While vaccination is the most effective intervention to limit debilitating infection, vaccines are not always effective in older people, and our knowledge of the cellular and molecular mechanisms that govern this are far from complete. In this study we set out to understand how the LN microenvironment contributes to this process. We demonstrated that the microenvironment was the key limiting factor for GC initiation, and that MAdCAM-1-expressing lymphoid stromal cells were particularly impaired in their capacity to respond to immunization. We dissected the MAdCAM-1$^+$ stromal cell response to immunization, highlighting global cellular and transcriptional changes that occurred within days of immunization, which were almost completely absent in cells obtained from aged mice. We demonstrated that MAdCAM-1$^+$ stromal cell responsiveness was enhanced by targeting the TLR4 pathway, offering proof-of-concept that lymphoid stromal cells can be rejuvenated in an aged vaccination setting via targeted adjuvant selection. We further showed that this enhanced stromal cell response correlated with improved initiation of GC responses, but that this did not necessarily enhance bone marrow ASCs or serum antibody titer, in agreement with previous work showing that the aged bone marrow microenvironment is poorly supportive of plasma cell maintenance (*57*).

The human LN becomes increasingly disrupted with advancing age, and the GC is particularly affected: both the number of GCs and the size of each GC is reduced in LNs obtained from older humans (*58-61*). Reduction in the size of the GC response with age is associated with poor protective immunity in infections and vaccine settings (*2-4*). Understanding the fundamental age-associated mechanisms that drive this response are critical to inform vaccine design to induce optimal protective immunity in older individuals. Our parabiosis studies demonstrated that the age of the LN microenvironment was the primary driver of poor vaccine-induced GC formation in aging. This defect was likely

intrinsic to the microenvironment, as the poor T cell immigration and survival that is observed in aged LNs is not rejuvenated by circulatory factors in heterochronic parabiosis (*62*), suggesting a key role for the resident stroma in controlling this phenomenon. Lymphoid stromal cells dynamically respond to immune challenge to support the development of immune responses (*18-20*). Aging impairs the capacity of FRCs, a heterogeneous population of $Pdpn^{+}CD31^{-}CD45^{-}$ stromal cells in the LN, to respond to immune challenge (*38*), potentially impacting on the kinetics of the immune response to infection. Aging also diminishes the expansion and functional capacity of FDCs to support GC formation (*39, 63-65*). Our work extends these findings as we demonstrated that MAdCAM-1^{+} lymphoid stromal cells underwent a transcriptional and phenotypic shift in response to immunization, and that this response was markedly impaired in aged mice. Our heterochronic parabiosis studies showed that the MAdCAM-1^{+} lymphoid stromal cell response was not rejuvenated by the presence of circulatory cells derived from younger adult mice, thus the responsiveness of MAdCAM-1^{+} lymphoid stromal cells to immunization may be cell autonomous.

Numerous studies have shown that lymphoid stromal cells respond to immune challenge (*20-22*), but few studies have investigated the specific cellular drivers of this response. Our data demonstrated that TLR4-stimulation, either through LPS or the TLR4-stimulating adjuvant, GLA-SE, significantly enhanced the activation and proliferation of MAdCAM-1^{+} lymphoid stromal cells relative to that induced by aluminum salt-based adjuvants. DCs are important in driving lymphoid stromal cell responses (*18, 19*); our data supported these findings, and also suggested that the response of MAdCAM-1^{+} lymphoid stromal cells to immunization may be more nuanced than previously thought. Their proliferation was dependent on TLR4 expression by hematopoietic cells, suggesting that the signal to enter cell cycle is delivered by TLR4-activated DCs or macrophages. In comparison, the activated phenotype of MAdCAM-1^{+} lymphoid stromal cells, as measured by high expression of Pdpn and VCAM-1, could be directly induced by stromal cell-expressed TLR4. This may be particularly relevant in aging,

as the response to TLR4 stimulation is reduced in macrophages (*66*). Pdpn and VCAM-1 have immunologically relevant functions that may promote the vaccine response in aging. Pdpn influences DC arrest and T cell activation (*67*) and also promotes immune-stromal crosstalk (*18, 19*), while the upregulation of VCAM-1 may promote DC recruitment to the LN, as has been recently shown for lymphatic endothelial cells (*68*). Responses to TLR4 ligands are described in other lymphoid stromal cells. Gut-associated FRC-like cells respond directly to TLR signaling, promoting the initiation of immunity to gut infection (*69*), while signaling via TLR4 drives the maturation and expansion of FDCs (*70, 71*), exemplified by upregulation of the adhesion molecules ICAM-1 and VCAM-1 (*72*). Since GLA-SE accumulates in the SCS (*73*), it is tempting to speculate that MAdCAM-1$^+$ lymphoid stromal cells located at the SCS directly sense TLR ligands in the adjuvant, leading to their enhanced activation, the effects of which could be twofold. They could be promoting DC recruitment to and arrest within the LN, leading to increased T cell activation, or they could be driving the differentiation of MRCs into FDCs (*37*). These effects may lead to accelerated initiation of the GC response, and our data showed that GLA-SE-adjuvanted immunization accelerated GC formation. GC-phenotype B cells and serum antigen-specific IgG detected after four days in younger adult mice, something not observed in AL007-adjuvanted immunization. While we cannot exclude a role for direct TLR4 signaling on FDCs augmenting their number and/or function, future studies using lymphoid stromal cell subset specific-targeting transgenic mouse models will clarify how different stromal cell subsets coordinate the adaptive immune response to immunization.

Our study demonstrated that MAdCAM-1$^+$ lymphoid stromal cells underwent substantial cellular and molecular changes early after NP-KLH+Alum immunization. The MAdCAM-1$^+$ lymphoid stromal cell response was much lower in aged mice which could be partially overcome by targeting the TLR4 pathway during vaccination. Our work highlights that the mechanism of action of adjuvants is not limited to an effect on inflammation and/or

immunity. Further study of how different adjuvants alter the stromal cell network and the impact immunity will offer insight into rational vaccine design to improve vaccine responses in older individuals.

Materials and Methods

Mice

C57BL/6, Balb/c, CD45.1^{+} C57BL/6.SJL, *Tlr4*$^{-/-}$ and *Il33*$^{cit/cit}$ mice were bred and housed in the Babraham Institute Biological Support Unit, MRC-LMB Ares unit or at the Animal Research Centre, University of Leuven, Belgium. Mice were housed under specific pathogen-free conditions and experiments conducted in accordance with UK home office and EU guidelines. Further details are available in the supplemental material.

Immunizations and parabiosis

Mice were immunized subcutaneously on the flank with 50μg of NP-KLH (Biosearch technologies, #N-5060) in Imject Alum (ThermoFisher Scientific, #77161), Imject Alum + 5μg LPS (Sigma, #L3102), or GLA-SE or Alhydrogel (AL007) (both from IDRI). Inguinal LNs were harvested and processed for analysis. Parabiosis was conducted essentially as described (*40, 74, 75*). Surgery was conducted under inhalation anesthesia according to LASA Dhiel guidelines. Three weeks after surgery, mice were immunized as above on the outer flanks and LNs analyzed on day seven. Further details are available in the supplemental material.

Cell isolation and flow cytometry

Stromal cells were released by enzymatic digestion essentially as described (*17, 76*) and suspensions were passed through a 70μm mesh prior to staining. For analysis of GC B cells, LNs were forced through a 40μm mesh in PBS containing 2% FCS or were analyzed from single cell suspensions prepared by enzymatic digestion. Cells were stained using cocktails of antibodies following Fc blocking. Samples were acquired on a BD LSRFortessa (BD Biosciences) harboring 355, 405, 488, 561 and 640nm lasers and analyzed using FlowJo software (TreeStar). Further details are available in the supplemental material.

Immunofluorescence microscopy

LNs were immersion-fixed in periodate-lysine-paraformaldehyde for five hours at 4°C, washed, cryoprotected in 30% sucrose (Sigma, #S0389) and embedded in optimal cutting temperature medium (VWR, #25608-930). Tissues sections were blocked and stained with antibodies and data collected as outlined in the supplemental material. Images were analyzed and compiled using Fiji software (National Institutes of Health).

RNA sequencing and analysis

Stromal cells were released from LNs by enzymatic digestion as described above and hematopoietic cells were depleted using anti-CD45 microbeads (Miltenyi Biotec, 130-052-301). MAdCAM-1$^+$ lymphoid stromal cells (MAdCAM-1$^+$CD21/35$^-$Pdpn$^+$CD31$^-$CD45$^-$) or FDCs (CD21/35$^+$Pdpn$^+$CD31$^-$CD45$^-$) were sorted directly into 8.5μL of lysis buffer. We performed sequencing on five biological replicates for each group; one aged unimmunized FDC samples was excluded from analysis as it failed post-processing QC, leaving four biological replicates in this group.

cDNA from sorted cells was generated using the SMART-Seq v4 Ultra low input RNA kit (Clontech, #634890) and libraries prepared with 400pg of cDNA per sample using the Illumina Nextera XT kit (#FC-131-1096). Samples were sequenced on a HiSeq 2500 (Illumina, v4 chemistry) as 100bp single-end reads. Analysis was performed using the SeqMonk software package (Babraham Institute, https://www.bioinformatics.babraham.ac.uk/projects/seqmonk/, version 1.47.1), as outlined in the supplemental materials.

Bone marrow chimeras

To generate bone marrow chimeras, recipient mice (CD45.1$^+$ B6, CD45.2$^+$ B6 or CD45.2$^+$ *Tlr4*$^{-/-}$) were irradiated with 800-1000rad in two doses using a Caesium-137 source using an

IBL 437C Irradiator. Recipient mice were reconstituted intravenously with 2-5x10^6 bone marrow donor cells, obtained from congenically distinct mice (CD45.1$^+$ B6, CD45.2$^+$ B6 or CD45.2$^+$ *Tlr4*$^{-/-}$). Chimeric mice were administered neomycin sulfate in drinking water for four weeks after reconstitution. Successful chimerism was determined by tail bleed at six weeks, and mice were immunized at least eight weeks after reconstitution for use in experiments.

Enzyme-linked immunospot (ELISpot) assay and Enzyme-linked immunosorbent assay (ELISA)

ELISpots and ELISAs were performed using NP20-BSA or NP2-BSA to stimulate bone marrow cells or capture antibodies; IgG was detected using goat anti-mouse IgG (1:8000, Sigma-Aldrich). Further details are available in the supplemental material.

Statistics

Experiments were repeated a minimum of two times; figure legends indicate where independent experiments were combined. Data were analyzed and visualized using Prism 9 (GraphPad). Statistical significance was determined using one and two-way ANOVA tests with Holm-Sidâk's or Sidâk's post-hoc corrections, Mann Whitney rank test, or multiple unpaired t-tests as specified in the figure legends. Groups were deemed significantly different when p-values <0.05. In graphs, each data point represents a biological replicate and lines indicate the median.

Supplementary Materials

Figure S1. Cellularity in younger adult and aged LNs during immunization.

Figure S2. Sort profiles for RNA sequencing and immunofluorescence imaging of MAdCAM-1 expression after immunization.

Figure S3. MAdCAM-1$^+$ lymphoid stromal cell and FDC identity and differential gene expression, as determined by RNA sequencing.

Figure S4. IL-33 expression by MAdCAM-1$^+$ lymphoid stromal cells is increased after Alum-adjuvanted immunization, but does not affect the GC response.

Figure S5. Lack of type I IFN signaling does not impact the MAdCAM-1$^+$ lymphoid stromal cell response to immunization.

Figure S6. Targeting TLR4 boosts the MAdCAM-1$^+$ lymphoid stromal cell and GC response to immunization, and TLR4 expression by immune cells promotes MAdCAM-1$^+$ lymphoid stromal cell activation.

Figure S7. TLR4-adjuvanted vaccination boosts the MAdCAM-1$^+$ lymphoid stromal cell and GC response in aging.

Table S1. Raw data file

References and notes

1. E. Montecino-Rodriguez, B. Berent-Maoz, K. Dorshkind, Causes, consequences, and reversal of immune system aging. *J Clin Invest* **123**, 958-965 (2013).
2. A. Ciabattini, C. Nardini, F. Santoro, P. Garagnani, C. Franceschi, D. Medaglini, Vaccination in the elderly: The challenge of immune changes with aging. *Semin Immunol* **40**, 83-94 (2018).
3. K. Goodwin, C. Viboud, L. Simonsen, Antibody response to influenza vaccination in the elderly: a quantitative review. *Vaccine* **24**, 1159-1169 (2006).
4. T. M. Govaert, C. T. Thijs, N. Masurel, M. J. Sprenger, G. J. Dinant, J. A. Knottnerus, The efficacy of influenza vaccination in elderly individuals. A randomized double-blind placebo-controlled trial. *JAMA* **272**, 1661-1665 (1994).
5. B. Weinberger, B. Grubeck-Loebenstein, Vaccines for the elderly. *Clin Microbiol Infect* **18 Suppl 5**, 100-108 (2012).
6. F. J. Weisel, G. V. Zuccarino-Catania, M. Chikina, M. J. Shlomchik, A Temporal Switch in the Germinal Center Determines Differential Output of Memory B and Plasma Cells. *Immunity* **44**, 116-130 (2016).
7. M. Stebegg, S. D. Kumar, A. Silva-Cayetano, V. R. Fonseca, M. A. Linterman, L. Graca, Regulation of the Germinal Center Response. *Front Immunol* **9**, 2469 (2018).
8. A. E. Denton, M. A. Linterman, Stromal networking: cellular connections in the germinal centre. *Curr Opin Immunol* **45**, 103-111 (2017).
9. J. L. Lee, M. A. Linterman, Mechanisms underpinning poor antibody responses to vaccines in ageing. *Immunol Lett* **241**, 1-14 (2022).
10. X. Yang, J. Stedra, J. Cerny, Relative contribution of T and B cells to hypermutation and selection of the antibody repertoire in germinal centers of aged mice. *J Exp Med* **183**, 959-970 (1996).
11. J. S. Lefebvre, A. R. Masters, J. W. Hopkins, L. Haynes, Age-related impairment of humoral response to influenza is associated with changes in antigen specific T follicular helper cell responses. *Sci Rep* **6**, 25051 (2016).
12. M. Stebegg, A. Bignon, D. L. Hill, A. Silva-Cayetano, C. Krueger, I. Vanderleyden, S. Innocentin, L. Boon, J. Wang, M. S. Zand, J. Dooley, J. Clark, A. Liston, E. Carr, M. A. Linterman, Rejuvenating conventional dendritic cells and T follicular helper cell formation after vaccination. *Elife* **9**, (2020).
13. D. L. Hill, C. E. Whyte, S. Innocentin, J. L. Lee, J. Dooley, J. Wang, E. A. James, J. C. Lee, W. W. Kwok, M. S. Zand, A. Liston, E. J. Carr, M. A. Linterman, Impaired HA-specific T follicular helper cell and antibody responses to influenza vaccination are linked to inflammation in humans. *Elife* **10**, (2021).
14. S. M. Eaton, E. M. Burns, K. Kusser, T. D. Randall, L. Haynes, Age-related defects in CD4 T cell cognate helper function lead to reductions in humoral responses. *J Exp Med* **200**, 1613-1622 (2004).
15. I. Cinti, A. E. Denton, Lymphoid stromal cells—more than just a highway to humoral immunity. *Oxford Open Immunology* **2**, (2021).
16. V. Cremasco, M. C. Woodruff, L. Onder, J. Cupovic, J. M. Nieves-Bonilla, F. A. Schildberg, J. Chang, F. Cremasco, C. J. Harvey, K. Wucherpfennig, B. Ludewig, M. C. Carroll, S. J. Turley, B cell homeostasis and follicle confines are governed by fibroblastic reticular cells. *Nat Immunol* **15**, 973-981 (2014).
17. A. E. Denton, E. W. Roberts, M. A. Linterman, D. T. Fearon, Fibroblastic reticular cells of the lymph node are required for retention of resting but not activated CD8+ T cells. *Proc Natl Acad Sci U S A* **111**, 12139-12144 (2014).
18. S. E. Acton, A. J. Farrugia, J. L. Astarita, D. Mourao-Sa, R. P. Jenkins, E. Nye, S. Hooper, J. van Blijswijk, N. C. Rogers, K. J. Snelgrove, I. Rosewell, L. F. Moita, G.

Stamp, S. J. Turley, E. Sahai, C. Reis e Sousa, Dendritic cells control fibroblastic reticular network tension and lymph node expansion. *Nature* **514**, 498-502 (2014).
19. J. L. Astarita, V. Cremasco, J. Fu, M. C. Darnell, J. R. Peck, J. M. Nieves-Bonilla, K. Song, Y. Kondo, M. C. Woodruff, A. Gogineni, L. Onder, B. Ludewig, R. M. Weimer, M. C. Carroll, D. J. Mooney, L. Xia, S. J. Turley, The CLEC-2-podoplanin axis controls the contractility of fibroblastic reticular cells and lymph node microarchitecture. *Nat Immunol* **16**, 75-84 (2015).
20. J. L. Gregory, A. Walter, Y. O. Alexandre, J. L. Hor, R. Liu, J. Z. Ma, S. Devi, N. Tokuda, Y. Owada, L. K. Mackay, G. K. Smyth, W. R. Heath, S. N. Mueller, Infection Programs Sustained Lymphoid Stromal Cell Responses and Shapes Lymph Node Remodeling upon Secondary Challenge. *Cell Rep* **18**, 406-418 (2017).
21. D. Malhotra, A. L. Fletcher, J. Astarita, V. Lukacs-Kornek, P. Tayalia, S. F. Gonzalez, K. G. Elpek, S. K. Chang, K. Knoblich, M. E. Hemler, M. B. Brenner, M. C. Carroll, D. J. Mooney, S. J. Turley, C. Immunological Genome Project, Transcriptional profiling of stroma from inflamed and resting lymph nodes defines immunological hallmarks. *Nat Immunol* **13**, 499-510 (2012).
22. C. Y. Yang, T. K. Vogt, S. Favre, L. Scarpellino, H. Y. Huang, F. Tacchini-Cottier, S. A. Luther, Trapping of naive lymphocytes triggers rapid growth and remodeling of the fibroblast network in reactive murine lymph nodes. *Proc Natl Acad Sci U S A* **111**, E109-118 (2014).
23. D. Aw, L. Hilliard, Y. Nishikawa, E. T. Cadman, R. A. Lawrence, D. B. Palmer, Disorganization of the splenic microanatomy in ageing mice. *Immunology* **148**, 92-101 (2016).
24. B. R. Becklund, J. F. Purton, C. Ramsey, S. Favre, T. K. Vogt, C. E. Martin, D. S. Spasova, G. Sarkisyan, E. LeRoy, J. T. Tan, H. Wahlus, B. Bondi-Boyd, S. A. Luther, C. D. Surh, The aged lymphoid tissue environment fails to support naive T cell homeostasis. *Sci Rep* **6**, 30842 (2016).
25. J. S. Lefebvre, A. C. Maue, S. M. Eaton, P. A. Lanthier, M. Tighe, L. Haynes, The aged microenvironment contributes to the age-related functional defects of CD4 T cells in mice. *Aging Cell* **11**, 732-740 (2012).
26. V. M. Turner, N. A. Mabbott, Influence of ageing on the microarchitecture of the spleen and lymph nodes. *Biogerontology* **18**, 723-738 (2017).
27. H. L. Thompson, M. J. Smithey, C. D. Surh, J. Nikolich-Zugich, Functional and Homeostatic Impact of Age-Related Changes in Lymph Node Stroma. *Front Immunol* **8**, 706 (2017).
28. J. M. Richner, G. B. Gmyrek, J. Govero, Y. Tu, G. J. van der Windt, T. U. Metcalf, E. K. Haddad, J. Textor, M. J. Miller, M. S. Diamond, Age-Dependent Cell Trafficking Defects in Draining Lymph Nodes Impair Adaptive Immunity and Control of West Nile Virus Infection. *PLoS Pathog* **11**, e1005027 (2015).
29. A. R. Masters, E. R. Jellison, L. Puddington, K. M. Khanna, L. Haynes, Attrition of T Cell Zone Fibroblastic Reticular Cell Number and Function in Aged Spleens. *Immunohorizons* **2**, 155-163 (2018).
30. X. Wang, B. Cho, K. Suzuki, Y. Xu, J. A. Green, J. An, J. G. Cyster, Follicular dendritic cells help establish follicle identity and promote B cell retention in germinal centers. *J Exp Med* **208**, 2497-2510 (2011).
31. C. D. Allen, J. G. Cyster, Follicular dendritic cell networks of primary follicles and germinal centers: phenotype and function. *Semin Immunol* **20**, 14-25 (2008).
32. O. Bannard, R. M. Horton, C. D. Allen, J. An, T. Nagasawa, J. G. Cyster, Germinal center centroblasts transition to a centrocyte phenotype according to a timed program and depend on the dark zone for effective selection. *Immunity* **39**, 912-924 (2013).

33. L. B. Rodda, O. Bannard, B. Ludewig, T. Nagasawa, J. G. Cyster, Phenotypic and Morphological Properties of Germinal Center Dark Zone Cxcl12-Expressing Reticular Cells. *J Immunol* **195**, 4781-4791 (2015).
34. N. B. Pikor, U. Morbe, M. Lutge, C. Gil-Cruz, C. Perez-Shibayama, M. Novkovic, H. W. Cheng, C. Nombela-Arrieta, T. Nagasawa, M. A. Linterman, L. Onder, B. Ludewig, Remodeling of light and dark zone follicular dendritic cells governs germinal center responses. *Nat Immunol*, (2020).
35. T. Katakai, Marginal reticular cells: a stromal subset directly descended from the lymphoid tissue organizer. *Front Immunol* **3**, 200 (2012).
36. T. Katakai, H. Suto, M. Sugai, H. Gonda, A. Togawa, S. Suematsu, Y. Ebisuno, K. Katagiri, T. Kinashi, A. Shimizu, Organizer-like reticular stromal cell layer common to adult secondary lymphoid organs. *J Immunol* **181**, 6189-6200 (2008).
37. M. Jarjour, A. Jorquera, I. Mondor, S. Wienert, P. Narang, M. C. Coles, F. Klauschen, M. Bajenoff, Fate mapping reveals origin and dynamics of lymph node follicular dendritic cells. *J Exp Med* **211**, 1109-1122 (2014).
38. A. R. Masters, A. Hall, J. M. Bartley, S. R. Keilich, E. C. Lorenzo, E. R. Jellison, L. Puddington, L. Haynes, Assessment of Lymph Node Stromal Cells as an Underlying Factor in Age-Related Immune Impairment. *J Gerontol A Biol Sci Med Sci* **74**, 1734-1743 (2019).
39. V. M. Turner, N. A. Mabbott, Structural and functional changes to lymph nodes in ageing mice. *Immunology* **151**, 239-247 (2017).
40. I. M. Conboy, M. J. Conboy, A. J. Wagers, E. R. Girma, I. L. Weissman, T. A. Rando, Rejuvenation of aged progenitor cells by exposure to a young systemic environment. *Nature* **433**, 760-764 (2005).
41. L. B. Rodda, E. Lu, M. L. Bennett, C. L. Sokol, X. Wang, S. A. Luther, B. A. Barres, A. D. Luster, C. J. Ye, J. G. Cyster, Single-Cell RNA Sequencing of Lymph Node Stromal Cells Reveals Niche-Associated Heterogeneity. *Immunity* **48**, 1014-1028 e1016 (2018).
42. Y. O. Alexandre, S. Devi, S. L. Park, L. K. Mackay, W. R. Heath, S. N. Mueller, Systemic Inflammation Suppresses Lymphoid Tissue Remodeling and B Cell Immunity during Concomitant Local Infection. *Cell Rep* **33**, 108567 (2020).
43. C. M. de Winde, S. Makris, L. J. Millward, J. A. Cantoral-Rebordinos, A. C. Benjamin, V. G. Martinez, S. E. Acton, Fibroblastic reticular cell response to dendritic cells requires coordinated activity of podoplanin, CD44 and CD9. *J Cell Sci* **134**, (2021).
44. C. Benezech, E. Mader, G. Desanti, M. Khan, K. Nakamura, A. White, C. F. Ware, G. Anderson, J. H. Caamano, Lymphotoxin-beta receptor signaling through NF-kappaB2-RelB pathway reprograms adipocyte precursors as lymph node stromal cells. *Immunity* **37**, 721-734 (2012).
45. C. S. Hardman, V. Panova, A. N. McKenzie, IL-33 citrine reporter mice reveal the temporal and spatial expression of IL-33 during allergic lung inflammation. *Eur J Immunol* **43**, 488-498 (2013).
46. H. I. Nakaya, T. Hagan, S. S. Duraisingham, E. K. Lee, M. Kwissa, N. Rouphael, D. Frasca, M. Gersten, A. K. Mehta, R. Gaujoux, G. M. Li, S. Gupta, R. Ahmed, M. J. Mulligan, S. Shen-Orr, B. B. Blomberg, S. Subramaniam, B. Pulendran, Systems Analysis of Immunity to Influenza Vaccination across Multiple Years and in Diverse Populations Reveals Shared Molecular Signatures. *Immunity* **43**, 1186-1198 (2015).
47. R. Spreafico, P. Ricciardi-Castagnoli, A. Mortellaro, The controversial relationship between NLRP3, alum, danger signals and the next-generation adjuvants. *Eur J Immunol* **40**, 638-642 (2010).
48. S. C. Eisenbarth, O. R. Colegio, W. O'Connor, F. S. Sutterwala, R. A. Flavell, Crucial role for the Nalp3 inflammasome in the immunostimulatory properties of aluminium adjuvants. *Nature* **453**, 1122-1126 (2008).

49. A. Iwasaki, S. B. Omer, Why and How Vaccines Work. *Cell* **183**, 290-295 (2020).
50. R. N. Coler, S. Bertholet, M. Moutaftsi, J. A. Guderian, H. P. Windish, S. L. Baldwin, E. M. Laughlin, M. S. Duthie, C. B. Fox, D. Carter, M. Friede, T. S. Vedvick, S. G. Reed, Development and characterization of synthetic glucopyranosyl lipid adjuvant system as a vaccine adjuvant. *PLoS One* **6**, e16333 (2011).
51. S. L. Baldwin, S. Bertholet, M. Kahn, I. Zharkikh, G. C. Ireton, T. S. Vedvick, S. G. Reed, R. N. Coler, Intradermal immunization improves protective efficacy of a novel TB vaccine candidate. *Vaccine* **27**, 3063-3071 (2009).
52. S. L. Baldwin, N. Shaverdian, Y. Goto, M. S. Duthie, V. S. Raman, T. Evers, F. Mompoint, T. S. Vedvick, S. Bertholet, R. N. Coler, S. G. Reed, Enhanced humoral and Type 1 cellular immune responses with Fluzone adjuvanted with a synthetic TLR4 agonist formulated in an emulsion. *Vaccine* **27**, 5956-5963 (2009).
53. R. N. Coler, T. A. Day, R. Ellis, F. M. Piazza, A. M. Beckmann, J. Vergara, T. Rolf, L. Lu, G. Alter, D. Hokey, L. Jayashankar, R. Walker, M. A. Snowden, T. Evans, A. Ginsberg, S. G. Reed, T.-S. Team, The TLR-4 agonist adjuvant, GLA-SE, improves magnitude and quality of immune responses elicited by the ID93 tuberculosis vaccine: first-in-human trial. *NPJ Vaccines* **3**, 34 (2018).
54. D. L. Hill, W. Pierson, D. J. Bolland, C. Mkindi, E. J. Carr, J. Wang, S. Houard, S. W. Wingett, R. Audran, E. F. Wallin, S. A. Jongo, K. Kamaka, M. Zand, F. Spertini, C. Daubenberger, A. E. Corcoran, M. A. Linterman, The adjuvant GLA-SE promotes human Tfh cell expansion and emergence of public TCRbeta clonotypes. *J Exp Med* **216**, 1857-1873 (2019).
55. S. L. Baldwin, F. C. Hsu, N. Van Hoeven, E. Gage, B. Granger, J. A. Guderian, S. E. Larsen, E. C. Lorenzo, L. Haynes, S. G. Reed, R. N. Coler, Improved Immune Responses in Young and Aged Mice with Adjuvanted Vaccines against H1N1 Influenza Infection. *Front Immunol* **9**, 295 (2018).
56. J. Falloon, F. Ji, C. Curtis, S. Bart, E. Sheldon, D. Krieger, F. Dubovsky, S. Lambert, T. Takas, T. Villafana, M. T. Esser, A phase 1a, first-in-human, randomized study of a respiratory syncytial virus F protein vaccine with and without a toll-like receptor-4 agonist and stable emulsion adjuvant. *Vaccine* **34**, 2847-2854 (2016).
57. S. Han, K. Yang, Z. Ozen, W. Peng, E. Marinova, G. Kelsoe, B. Zheng, Enhanced differentiation of splenic plasma cells but diminished long-lived high-affinity bone marrow plasma cells in aged mice. *J Immunol* **170**, 1267-1273 (2003).
58. J. Garatea-Crelgo, C. Gay-Escoda, B. Bermejo, R. Buenechea-Imaz, Morphological study of the parotid lymph nodes. *J Craniomaxillofac Surg* **21**, 207-209 (1993).
59. P. Luscieti, T. Hubschmid, H. Cottier, M. W. Hess, L. H. Sobin, Human lymph node morphology as a function of age and site. *J Clin Pathol* **33**, 454-461 (1980).
60. W. R. Pan, H. Suami, G. I. Taylor, Senile changes in human lymph nodes. *Lymphat Res Biol* **6**, 77-83 (2008).
61. I. Taniguchi, A. Sakurada, G. Murakami, D. Suzuki, M. Sato, G. I. Kohama, Comparative histology of lymph nodes from aged animals and humans with special reference to the proportional areas of the nodal cortex and sinus. *Ann Anat* **186**, 337-347 (2004).
62. J. S. Davies, H. L. Thompson, V. Pulko, J. Padilla Torres, J. Nikolich-Zugich, Role of Cell-Intrinsic and Environmental Age-Related Changes in Altered Maintenance of Murine T Cells in Lymphoid Organs. *J Gerontol A Biol Sci Med Sci* **73**, 1018-1026 (2018).
63. Y. Aydar, P. Balogh, J. G. Tew, A. K. Szakal, Age-related depression of FDC accessory functions and CD21 ligand-mediated repair of co-stimulation. *Eur J Immunol* **32**, 2817-2826 (2002).

64. Y. Aydar, P. Balogh, J. G. Tew, A. K. Szakal, Altered regulation of Fc gamma RII on aged follicular dendritic cells correlates with immunoreceptor tyrosine-based inhibition motif signaling in B cells and reduced germinal center formation. *J Immunol* **171**, 5975-5987 (2003).
65. Y. Aydar, P. Balogh, J. G. Tew, A. K. Szakal, Follicular dendritic cells in aging, a "bottle-neck" in the humoral immune response. *Ageing Res Rev* **3**, 15-29 (2004).
66. M. Renshaw, J. Rockwell, C. Engleman, A. Gewirtz, J. Katz, S. Sambhara, Cutting edge: impaired Toll-like receptor expression and function in aging. *J Immunol* **169**, 4697-4701 (2002).
67. S. E. Acton, J. L. Astarita, D. Malhotra, V. Lukacs-Kornek, B. Franz, P. R. Hess, Z. Jakus, M. Kuligowski, A. L. Fletcher, K. G. Elpek, A. Bellemare-Pelletier, L. Sceats, E. D. Reynoso, S. F. Gonzalez, D. B. Graham, J. Chang, A. Peters, M. Woodruff, Y. A. Kim, W. Swat, T. Morita, V. Kuchroo, M. C. Carroll, M. L. Kahn, K. W. Wucherpfennig, S. J. Turley, Podoplanin-rich stromal networks induce dendritic cell motility via activation of the C-type lectin receptor CLEC-2. *Immunity* **37**, 276-289 (2012).
68. J. Arasa, V. Collado-Diaz, I. Kritikos, J. D. Medina-Sanchez, M. C. Friess, E. C. Sigmund, P. Schineis, M. C. Hunter, C. Tacconi, N. Paterson, T. Nagasawa, F. Kiefer, T. Makinen, M. Detmar, M. Moser, T. Lammermann, C. Halin, Upregulation of VCAM-1 in lymphatic collectors supports dendritic cell entry and rapid migration to lymph nodes in inflammation. *J Exp Med* **218**, (2021).
69. C. Perez-Shibayama, C. Gil-Cruz, H. W. Cheng, L. Onder, A. Printz, U. Morbe, M. Novkovic, C. Li, C. Lopez-Macias, M. B. Buechler, S. J. Turley, M. Mack, C. Soneson, M. D. Robinson, E. Scandella, J. Gommerman, B. Ludewig, Fibroblastic reticular cells initiate immune responses in visceral adipose tissues and secure peritoneal immunity. *Sci Immunol* **3**, (2018).
70. A. Garin, M. Meyer-Hermann, M. Contie, M. T. Figge, V. Buatois, M. Gunzer, K. M. Toellner, G. Elson, M. H. Kosco-Vilbois, Toll-like receptor 4 signaling by follicular dendritic cells is pivotal for germinal center onset and affinity maturation. *Immunity* **33**, 84-95 (2010).
71. B. A. Heesters, K. van Megesen, I. Tomris, R. P. de Vries, G. Magri, H. Spits, Characterization of human FDCs reveals regulation of T cells and antigen presentation to B cells. *J Exp Med* **218**, (2021).
72. M. E. El Shikh, R. M. El Sayed, Y. Wu, A. K. Szakal, J. G. Tew, TLR4 on follicular dendritic cells: an activation pathway that promotes accessory activity. *J Immunol* **179**, 4444-4450 (2007).
73. A. L. Desbien, N. Dubois Cauwelaert, S. J. Reed, H. R. Bailor, H. Liang, D. Carter, M. S. Duthie, C. B. Fox, S. G. Reed, M. T. Orr, IL-18 and Subcapsular Lymph Node Macrophages are Essential for Enhanced B Cell Responses with TLR4 Agonist Adjuvants. *J Immunol* **197**, 4351-4359 (2016).
74. E. Bunster, R. K. Meyer, An improved method of parabiosis. *The Anatomical Record* **57**, 339-343 (1933).
75. D. E. Wright, A. J. Wagers, A. P. Gulati, F. L. Johnson, I. L. Weissman, Physiological migration of hematopoietic stem and progenitor cells. *Science* **294**, 1933-1936 (2001).
76. A. E. Denton, E. J. Carr, L. P. Magiera, A. J. B. Watts, D. T. Fearon, Embryonic FAP(+) lymphoid tissue organizer cells generate the reticular network of adult lymph nodes. *J Exp Med* **216**, 2242-2252 (2019).

Acknowledgements

The authors thank staff from the Biological Support Unit and the Flow Cytometry and Imaging Facilities at the Babraham Research Campus, and the joint LMS/NIHR Imperial Biomedical Research Centre Flow Cytometry Facility at Imperial College London for support. The authors thank Prof. Kiyoshi Takeda for *Tlr4*$^{-/-}$ mice.

Competing interests: The authors declare that they have no competing interests.

Funding

AED was supported by a Biotechnology and Biological Sciences Research Council Future Leader Fellowship (BB/N011740/1) and an MRC Career Development Award (MR/V009591/1), DLH was supported by a National Health and Medical Research Council Australia Early-Career Fellowship (APP1139911). This work was supported by an H2020 European Research Council grant to MAL (637801 TWILIGHT), a Biotechnology and Biological Sciences Research Council grants to MAL (BBS/E/B/000C0408 and BBS/E/B/000C0407), a European Research Council Consolidator grant to AL (TissueTreg), and a Biotechnology and Biological Sciences Research Council Campus Capability grant to the Babraham Institute. This research was funded in whole or in part by UKRI BBSRC and MRC, both cOAlition S organizations. The author will make the Author Accepted Manuscript (AAM) version available under a CC BY public copyright license.

Author contributions

AED designed the study, conducted experiments, analyzed results, acquired funding and wrote the manuscript. JD and DLH conducted experiments and provided scientific advice. IC, ASC, SFB, and SI performed experiments. EJC supervised data analysis and provided scientific advice. AJN provided reagents. AL supervised research and edited the manuscript. MAL designed the study, supervised research, acquired funding and wrote the manuscript. All authors read, edited, and approved the manuscript.

Data availability:

All data needed to evaluate the conclusions in the paper are present in the paper or the Supplementary Materials. RNA sequencing data has been deposited at the Gene Expression Omnibus, GSE150054

Figure Captions

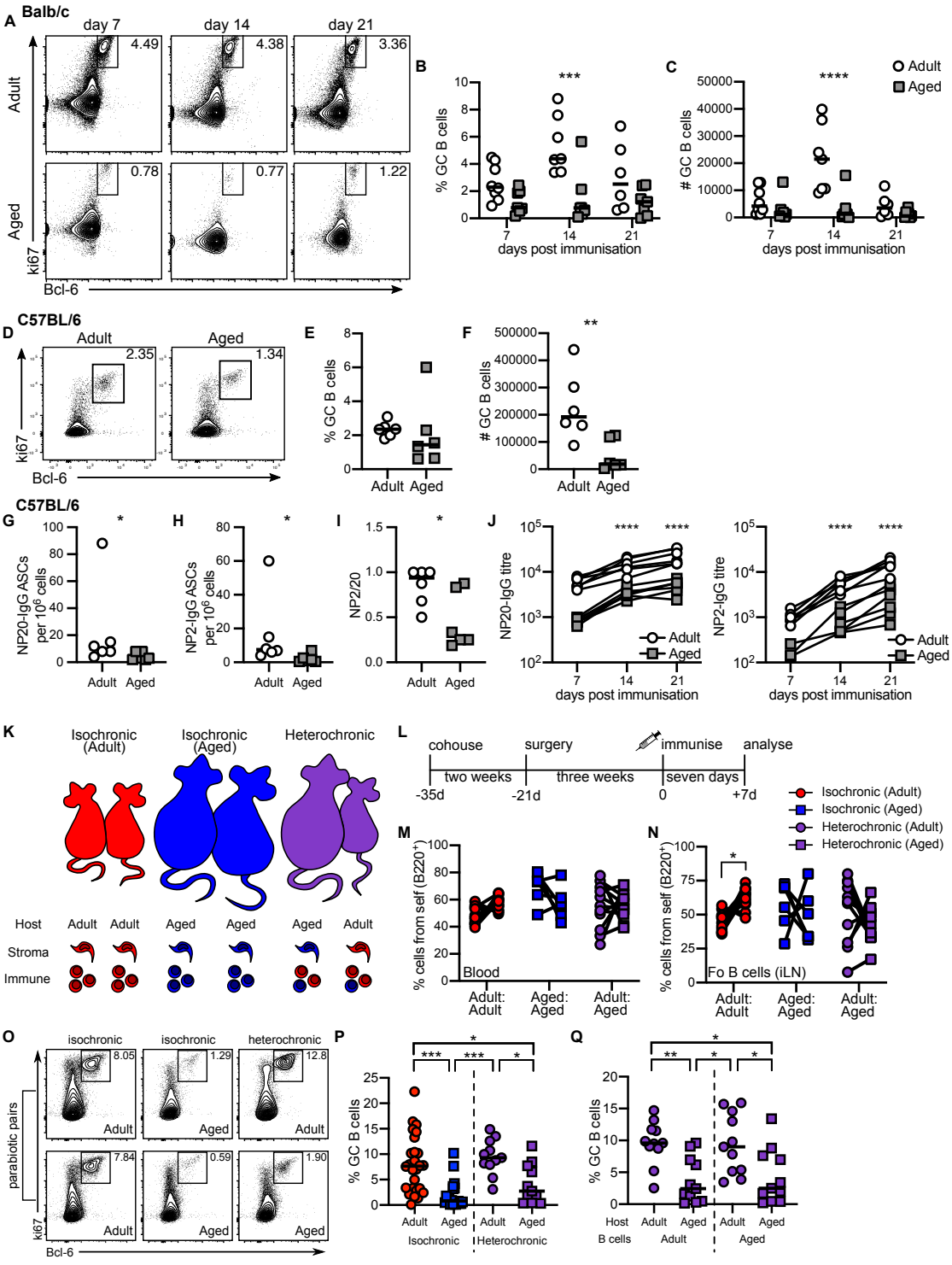

Figure 1. Age-associated defects in the GC response to immunization are driven by the microenvironment. (A-C) Adult (8-12week old) and aged (>98 week old) Balb/c mice were immunized subcutaneously with 50µg NP-KLH emulsified in Alum and the GC response was determined 7-21d later. Shown are representative flow cytometry profiles (A), and the

proportion (B) and absolute number (C) of ki67$^+$Bcl6$^+$ GC B cells. (D-F) Adult (8-12week old) and aged (>98 week old) C57BL/6 mice were immunized subcutaneously with 50μg NP-KLH emulsified in Alum and the GC response was determined 7d later. Shown are representative flow cytometry profiles (D), and the proportion (E) and absolute number (F) of ki67$^+$Bcl-6$^+$ GC B cells. (G-J) Adult (8-12week old) and aged (>98 week old) C57BL/6 mice were immunized subcutaneously with 50μg NP-KLH emulsified in Alum and the output of the GC response was determined 21d later. Shown are the number of low (G) and high (H) affinity IgG-producing antibody secreting cells (ASCs) in the bone marrow, and the ratio of high:low affinity ASCs (I). Serum low (NP20)- and high (NP2)-affinity antibody titres were determined seven, 14 and 21 days after immunisation in adult and aged mice (J). (K-Q) Heterochronic parabiosis was used to determine the role of the aged LN microenvironment in the generation of the GC response. Congenically distinct (CD45.1$^+$ or CD45.2$^+$) C57BL/6 mice were paired in isochronic (adult:adult, red; or aged:aged, blue) parabionts or heterochronic (adult:aged, purple) parabionts (K). Mouse pairs were cohoused for two weeks, then surgically joined; three weeks after surgery mice were immunized subcutaneously with 50μg NP-KLH emulsified in Alum on the outer flanks. Seven days after immunization the GC response was determined by flow cytometry (L). Blood B cell (M) and draining (d)LN non-GC B cell (N) chimerism were used to determine successful parabiosis. Mice with 40-80% self-derived B cells were used for subsequent analyses. The GC response was measured by ki67$^+$Bcl-6$^+$ staining (O), displayed as the proportion of B220$^+$ B cells (P). Within heterochronic parabionts, B cells were gated based on donor age using congenic markers, and their capacity to generate a GC response within adult or aged hosts was determined as a proportion of B220$^+$ B cells (Q). Data in (A-J) are representative of at least two independent experiments with 5-8 mice per group. Data in (K-Q) are combined from six separate experiments, using 4-20 mice per group (2-10 pairs). Data in (M, N) show individual mice with lines connecting paired blood samples. In (P, Q) each data point represents an individual mouse; individual mice from isochronic parabionts are represented as a single group.

Responses to immunization are deemed independent; blood and Fo B cell samples are paired. Each symbol represents a biological replicate and lines indicate the median. Statistical significance was determined using a two-way ANOVA with Sidâk's multiple comparison test (B,C, M, N), a Mann-Whitney rank test (E-I), a multiple unpaired t-test (J), or a one-way ANOVA with Holm-Sidâk's multiple comparison test (P, Q). * $p<0.05$, ** $p<0.01$ *** $p<0.001$ **** $p<0.0001$.

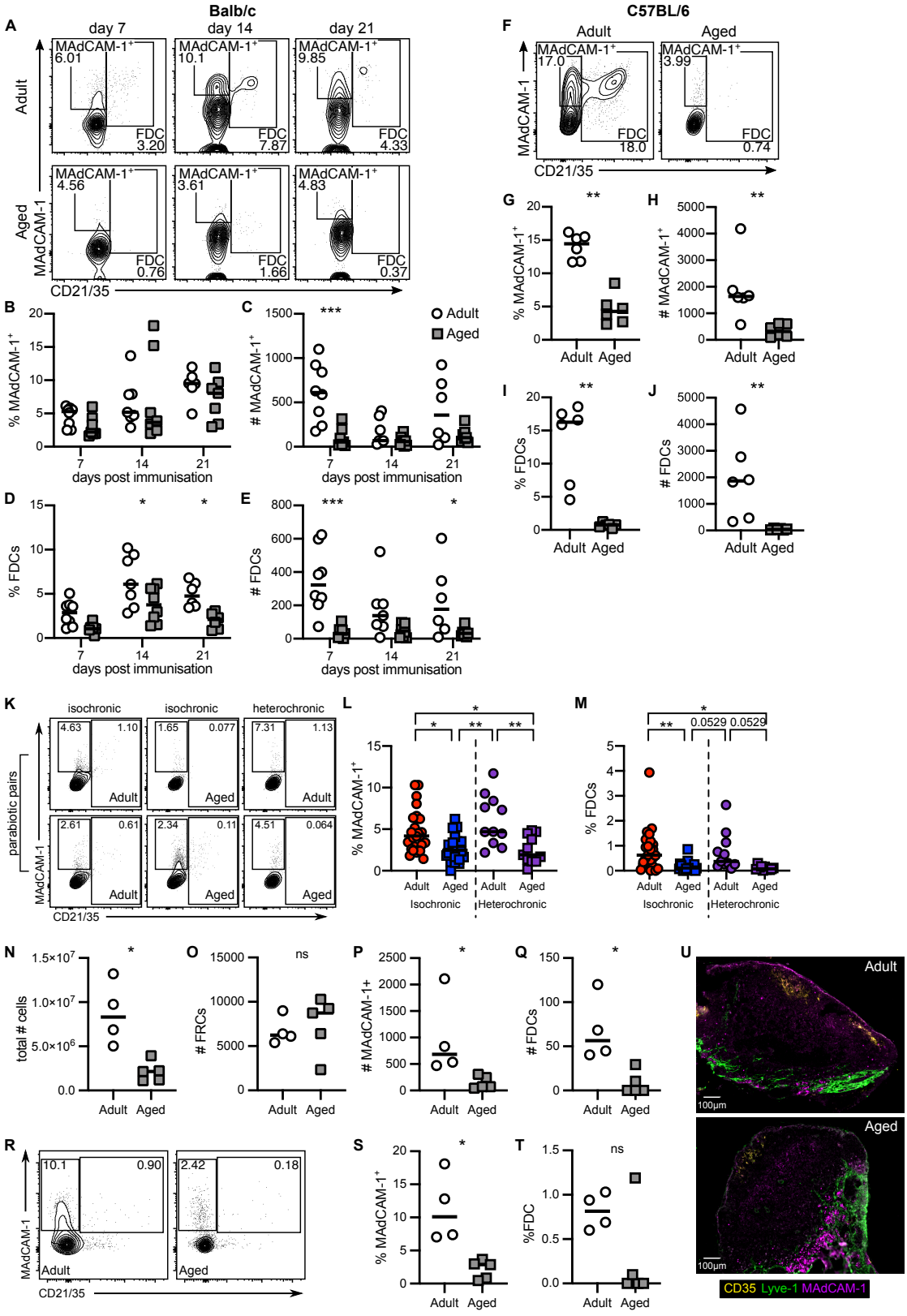

Figure 2. Lymphoid stromal cells fail to expand in response to immunization in aged mice. (A-E) Adult (8-12week old) and aged (>98 week old) Balb/c mice were immunized as described in Fig 1A-C and stromal cell responses were determined on d7-21. MAdCAM-1+

lymphoid stromal cells (MAdCAM-1$^+$CD21/35$^-$) and FDCs (CD21/35$^+$) were gated on CD45$^-$CD31$^-$Pdpn$^+$ stromal cells (A) and results are shown as the proportion of CD45$^-$CD31$^-$Pdpn$^+$ stromal cells (B, D) and absolute number (C, E). (F-J) Adult (8-12week old) and aged (>98 week old) C57BL/6 mice were immunized as described in Fig 1D-F and stromal cell responses were determined on d7. MAdCAM-1$^+$ lymphoid stromal cells and FDCs were gated on CD45$^-$CD31$^-$Pdpn$^+$ stromal cells (F) and data are shown as the proportion of CD31$^-$CD45$^-$Pdpn$^+$ stromal cells (G, I) and absolute number (H, J). (K-M) Heterochronic parabiosis was performed as in Fig 1K-L; the proportion of MAdCAM-1$^+$ lymphoid stromal cells and FDCs was determined as the proportion of CD45$^-$CD31$^-$Pdpn$^+$ stromal cells. Each symbol represents a biological replicate and lines indicate the median. (N-U) The number of different lymphoid stromal cells was determined in LNs from naïve younger adult and aged C57BL/6 mice. Shown are the total LN cellularity (N), the number of FRCs (CD31$^-$CD45$^-$Pdpn$^+$MAdCAM-1$^-$CD21/35$^-$) (O), MAdCAM-1$^+$ lymphoid stromal cells (P) and FDCs (Q), alongside gating for FDCs and MAdCAM-1$^+$ lymphoid stromal cells (R) and the proportion of MAdCAM-1$^+$ lymphoid stromal cells (S) and FDCs (T) amongst CD31$^-$CD45$^-$Pdpn$^+$ stromal cells. LNs from younger adult and aged C57BL/6 mice (U) were stained for MAdCAM-1 (magenta), Lyve-1 (green) and CD35 (yellow). Scale bars 100μm. Data in (A-J) and (N-U) are representative of at least two independent experiments with 4-8 mice per group. Data in (K-M) are combined from six separate experiments, using 4-20 mice per group (2-10 pairs). Individual mice from isochronic parabionts are represented as a single group and are regarded as independent. Statistical significance was determined using a two-way ANOVA with Sidâk's multiple comparison test (A-C), a Mann-Whitney rank test (F-J, N-T) or a one-way ANOVA with Holm-Sidâk's multiple comparison test (M, N). * $p<0.05$, **$p<0.01$ ***$p<0.001$ ****$p<0.0001$.

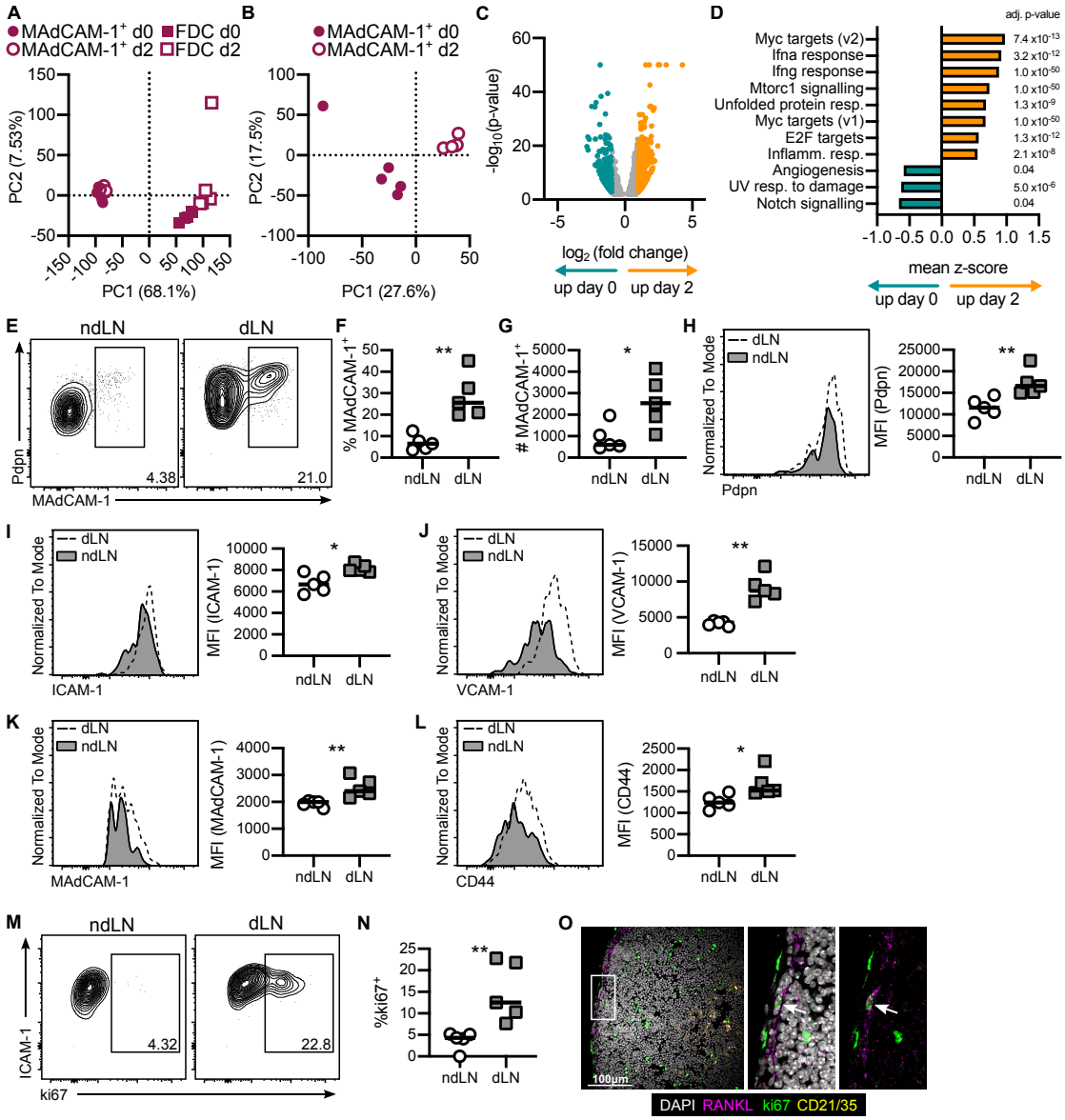

Figure 3. MAdCAM-1⁺ lymphoid stromal cells respond to NP-KLH+Alum immunization. (A) MAdCAM-1⁺ lymphoid stromal cells and FDCs were sort-purified from adult (8-12week old) naïve C57BL/6 mice and adult (8-12week old) C57BL/6 mice immunized two days prior with 50μg NP-KLH emulsified in Alum and subjected to bulk RNA sequencing. Principal component analysis (PCA) was conducted using the 1000 most variable genes. (B-D) Data from bulk sequencing of MAdCAM-1⁺ lymphoid stromal cells derived from naïve and immunized adult mice were re-analysed separately from that of FDCs. PCA analysis was conducted using the 1000 most variable genes (B). Differential gene expression between naïve and immunized MAdCAM-1⁺ lymphoid stromal cells was determined by DESeq2 and genes with expression differences with an absolute shrunken

log_2(fold change)>1 and an adjusted p value <0.05 were identified (C); orange = genes up-regulated after immunization, teal = genes up-regulated in naïve MAdCAM-1$^+$ lymphoid stromal cells. Gene set enrichment analysis was conducted using the Hallmark gene sets on all expressed genes (D). Gene sets were graphed based on z-score and the adjusted p-value is indicated; orange = gene sets up-regulated after immunization, teal = gene sets up-regulated in naïve MAdCAM-1$^+$ lymphoid stromal cells. (E-O) Adult (8-12week old) C57BL/6 mice were immunized subcutaneously with 50μg NP-KLH+Alum and the MAdCAM-1$^+$ lymphoid stromal cell response was determined four days later in the dLN compared to ndLN controls. MAdCAM-1$^+$ lymphoid stromal cells were measured as the proportion amongst CD45$^-$CD31$^-$CD21/35$^-$Pdpn$^+$ cells (E, F) and in absolute number (G). Cell surface phenotype was determined by measuring the MFI of antibody staining for Pdpn (H), ICAM-1 (I), VCAM-1 (J), MAdCAM-1 (K) and CD44 (L) on MAdCAM-1$^+$ lymphoid stromal cells. (M-O) MAdCAM-1$^+$ lymphoid stromal cell proliferation was determined four days after immunization in younger adult (8-12 week old) C57BL/6 mice. The proportion of proliferating MAdCAM-1$^+$ lymphoid stromal cells was determined using ki67 staining (M, N). MRC proliferation was confirmed with confocal microscopy (O), where cryosections of the dLN obtained four days after immunization were stained for ki67 (green), CD21/35 (yellow), RANKL (magenta) and DAPI (grey); scale bar 100μm. Arrow indicates ki67$^+$ MRC. Data in (E-O) are representative of at least three independent experiments with 4-6 mice per group. Statistical significance was determined using a Mann-Whitney rank test; *p<0.05 **p<0.01.

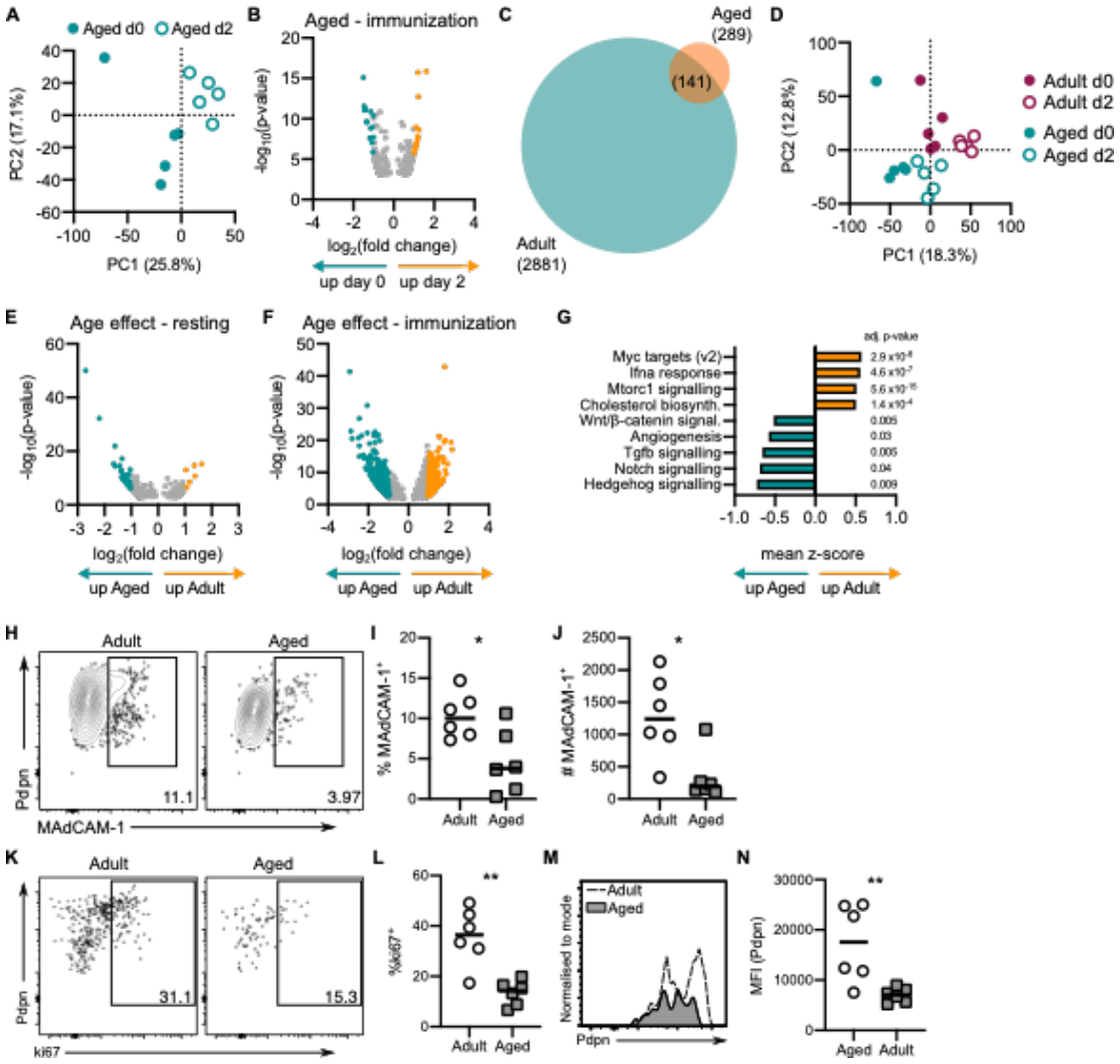

Figure 4. Aging impairs the MAdCAM-1⁺ lymphoid stromal cell response to Alum-adjuvanted immunization. (A-G) MAdCAM-1⁺ lymphoid stromal cells were sort-purified from aged (>98 week old) naïve C57BL/6 mice and aged (>98 week old) C57BL/6 mice immunized two days prior with 50µg NP-KLH emulsified in Alum and subjected to bulk RNA sequencing. PCA was conducted using the 1000 most variable genes (A). Differential gene expression between unimmunized and immunized aged MAdCAM-1⁺ lymphoid stromal cells was determined by DESeq2 and genes with significant expression differences ($p<0.05$) with an absolute shrunken $\log_2$(fold change)>1 were identified (B); orange = genes up-regulated after immunization, teal = genes up-regulated in naïve MAdCAM-1⁺ lymphoid stromal cells. The transcriptional changes induced after immunization were compared for adult (Fig 3 I-K, 2881 genes) and aged (289 genes) MAdCAM-1⁺ lymphoid stromal cells (C).

PCA of all naïve and immunized adult and aged MAdCAM-1$^+$ lymphoid stromal cell samples was conducted using the 1000 most variable genes (D). Differential gene expression between unimmunized adult and aged MAdCAM-1$^+$ lymphoid stromal cells was determined by DESeq2; genes with significant expression differences ($p<0.05$) and an absolute shrunken $\log_2$(fold change)>1 were identified; teal = genes up-regulated in aged, orange = genes up-regulated in adult. Differential gene expression between day two immunized adult and aged MAdCAM-1$^+$ lymphoid stromal cells was determined by DESeq2; genes with significant expression differences and an absolute shrunken $\log_2$(fold change)>1 were identified; teal = genes up-regulated in aged, orange = genes up-regulated in adult (F). Gene set enrichment analysis was conducted on MAdCAM-1$^+$ lymphoid stromal cells isolated from adult and aged mice two days after immunization using the Hallmark gene sets (G). Gene sets were graphed based on z-score and the adjusted p-value is indicated; teal = gene sets up-regulated in aged, orange = gene sets up-regulated in adult. (H-M) Adult (8-12week old) and aged (>98 week old) C57BL/6 mice were immunized with NP-KLH+Alum and the stromal cell response determined four days later. MAdCAM-1$^+$ lymphoid stromal cells were measured as the proportion of CD45$^-$CD31$^-$CD21/35$^-$Pdpn$^+$ stromal cells (H, I) and in absolute number (J). Proliferation was measured by ki67$^+$ staining (K, L). Pdpn expression by MAdCAM-1$^+$ lymphoid stromal cells was measured by flow cytometry (M-N). Data in (H-N) are representative of three independent experiments with 5-6 mice per group. Statistical significance was determined using a Mann-Whitney rank test, *$p<0.05$ **$p<0.01$.

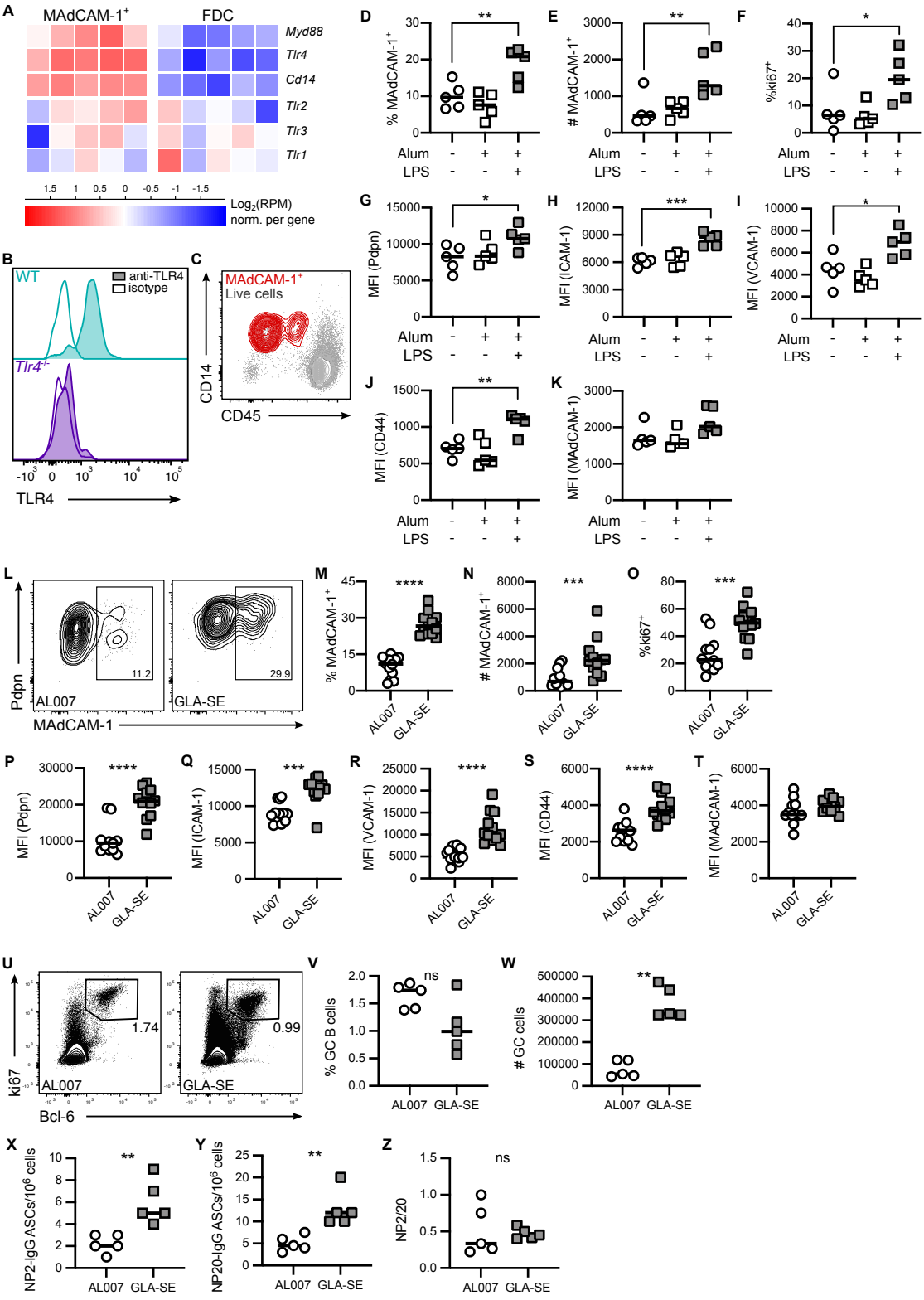

Figure 5. TLR4 stimulation promotes MAdCAM-1⁺ lymphoid stromal cells responses.

(A) RNA sequencing data from naïve younger adult (8-12week old) MAdCAM-1⁺ lymphoid stromal cells and FDCs were mined for the expression of toll-like receptor genes and downstream signalling elements associated with *Tlr4*, represented as log_2(RPM) counts

normalized per gene (n=5), as indicted by the color scale. (B) Protein staining for TLR4 was determined by flow cytometry, showing TLR4 (filled histogram) and isotype control (empty histogram) staining on MAdCAM-1$^+$ lymphoid stromal cells isolated from C57BL/6 and *Tlr4*$^{-/-}$ mice. (C) Protein staining for CD14 was determined by flow cytometry, showing MAdCAM-1$^+$ lymphoid stromal cells (red) overlaid with total live cells (grey). (D-K) Adult (8-12week old) C57BL/6 mice were administered PBS, Alum or 5μg LPS emulsified in Alum subcutaneously and the MAdCAM-1$^+$ lymphoid stromal cell response was determined four days later. The MAdCAM-1$^+$ lymphoid stromal cell response was measured as the proportion of MAdCAM-1$^+$ cells within the CD45$^-$CD31$^-$CD21/35$^-$Pdpn$^+$ population (D) and in absolute number (E). The proliferation (F) and upregulation of Pdpn (G), ICAM-1 (H), VCAM-1 (I), CD44 (J) and MAdCAM-1 (K), were also determined. (L-T) Adult (8-12 week old) C57BL/6 mice were administered 50μg NP-KLH in AL007 or GLA-SE and the MAdCAM-1$^+$ lymphoid stromal cell response was determined four days later. MAdCAM-1$^+$ lymphoid stromal cells were measured as the proportion of MAdCAM-1$^+$ cells amongst CD45$^-$CD31$^-$CD21/35$^-$Pdpn$^+$ stromal cells (L, M) and in absolute number (N). The proliferation of MAdCAM-1$^+$ lymphoid stromal cells was determined by ki67 expression (O) as was the upregulation of Pdpn (P), ICAM-1 (Q), VCAM-1 (R), CD44 (W) and MAdCAM-1 (T). (U-Z) Adult (8-12week old) C57BL/6 mice were administered 50μg NP-KLH in AL007 or GLA-SE and the GC response and output was determined 21 days later. Shown are gating of GC B cells (U), and both the proportion (V) and total number (W) of GC B cells in the dLN, alongside the number of high (X) and low (Y) affinity IgG-producing ASCs in bone marrow, and the ratio of high:low affinity ASCs (Z). Data in (B, C) are representative of at least three independent experiments. Data in (D-K) are representative of two independent experiments with four mice per group. Statistical significance was determined using a one-way ANOVA using Dunnett's multiple comparison test, with Alum and Alum+LPS groups compared to PBS. * $p<0.05$, ** $p<0.01$, *** $p<0.001$. Data in (M-Z) are representative of at least two

independent experiments with five mice per group. Statistical significance was determined using a Mann-Whitney rank test, *p<0.05, **p<0.01, ***p<0.001, ****p<0.0001.

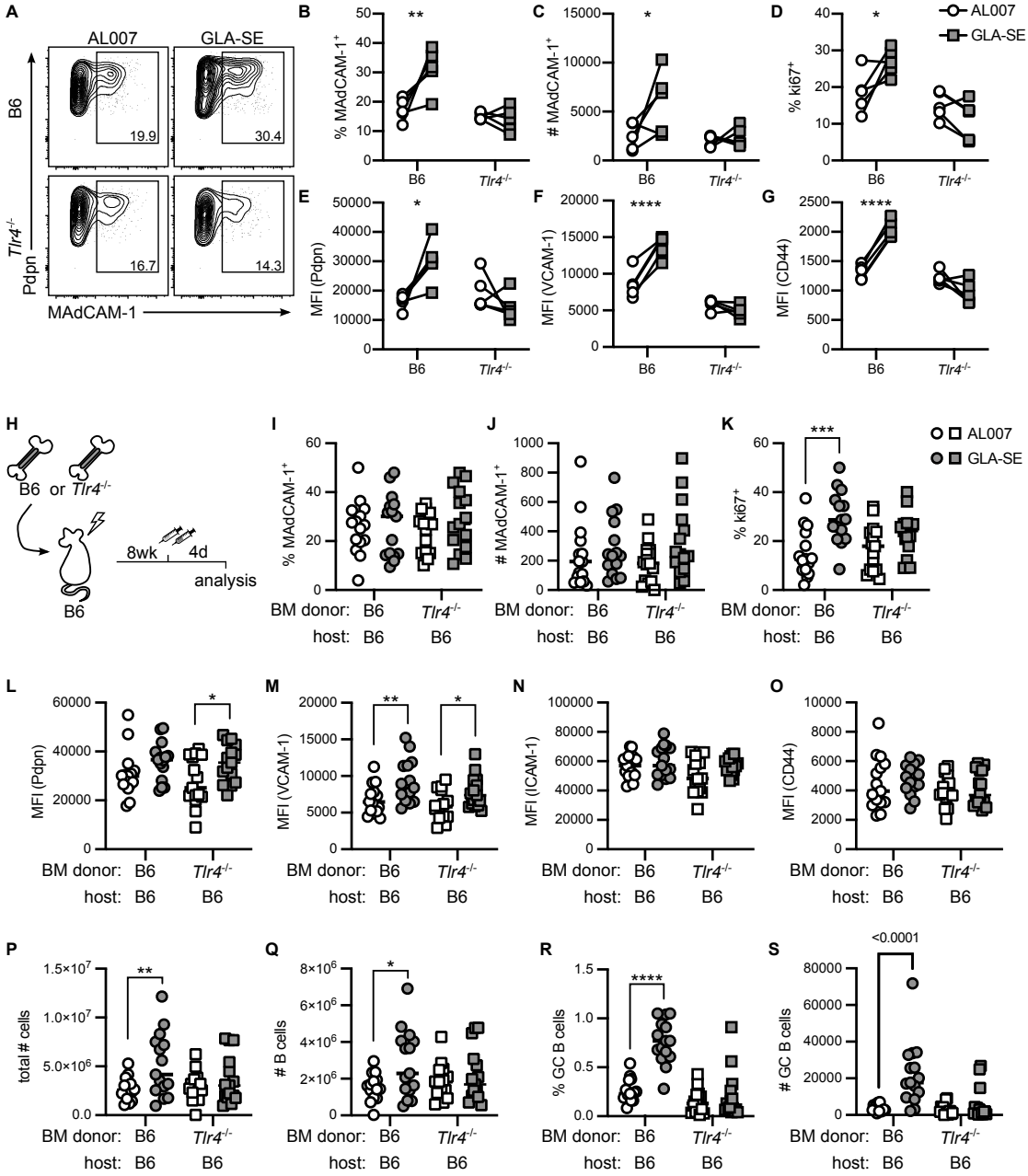

Figure 6. TLR4 expression by MAdCAM-1⁺ lymphoid stromal cells contributes to their activation in GLA-SE-adjuvanted immunization. (A-G) Adult (8-12 week old) C57BL/6 and *Tlr4*$^{-/-}$ mice were administered 50μg NP-KLH in AL007 or GLA-SE on opposing flanks and the MAdCAM-1⁺ lymphoid stromal cell response was determined four days later. MAdCAM-1⁺ lymphoid stromal cells, gated as MAdCAM-1⁺ amongst CD45⁻CD31⁻CD21/35⁻ Pdpn⁺ cells (A), were measured as both by proportion B) and in absolute number (C).

MAdCAM-1$^+$ lymphoid stromal cell responsiveness was measured by proliferation (D) and upregulation of cell surface markers Pdpn (E), VCAM-1 (F) and CD44 (G). (H-S) Adult (8-12 week old) C57BL/6 or *Tlr4*$^{-/-}$ bone marrow donors were used to reconstitute irradiated CD45.1$^+$ C57BL/6.SJL hosts to generate chimeric animals in which TLR4 expression is restricted to radioresistant lymphoid stromal cells. Eight weeks after reconstitution, mice were administered 50μg NP-KLH in AL007 or GLA-SE on opposing flanks and the MAdCAM-1$^+$ lymphoid stromal cell and GC responses were determined four days later (H). MAdCAM-1$^+$ lymphoid stromal cell responses were measured by proportion of CD31$^-$CD45$^-$Pdpn$^+$ lymphoid fibroblasts (I) and in absolute number (J). MAdCAM-1$^+$ lymphoid stromal cell proliferation was measured by ki67 staining (K) and their phenotype was determined by upregulation of cell surface markers: Pdpn (L), VCAM-1 (M), ICAM-1 (N) and CD44 (O). The GC response was measured by the total LN cellularity (P), the total number of B cells (Q) and the proportion (R) and total number (S) of GC B cells. Data in (A-G) are representative of at least two independent experiments with five mice per group. Paired immunizations in individual mice are linked by a line. Data in (H-S) are combined of two independent experiments, with 7-8 mice per group in each experiment. Statistical significance was determined using a paired two-way ANOVA (B-G) or a one-way ANOVA (M-T) with Sidâk's multiple comparison test, comparing AL007 to GLA-SE within each chimera group, * $p<0.05$, ** $p<0.01$, *** $p<0.001$, **** $p<0.0001$.

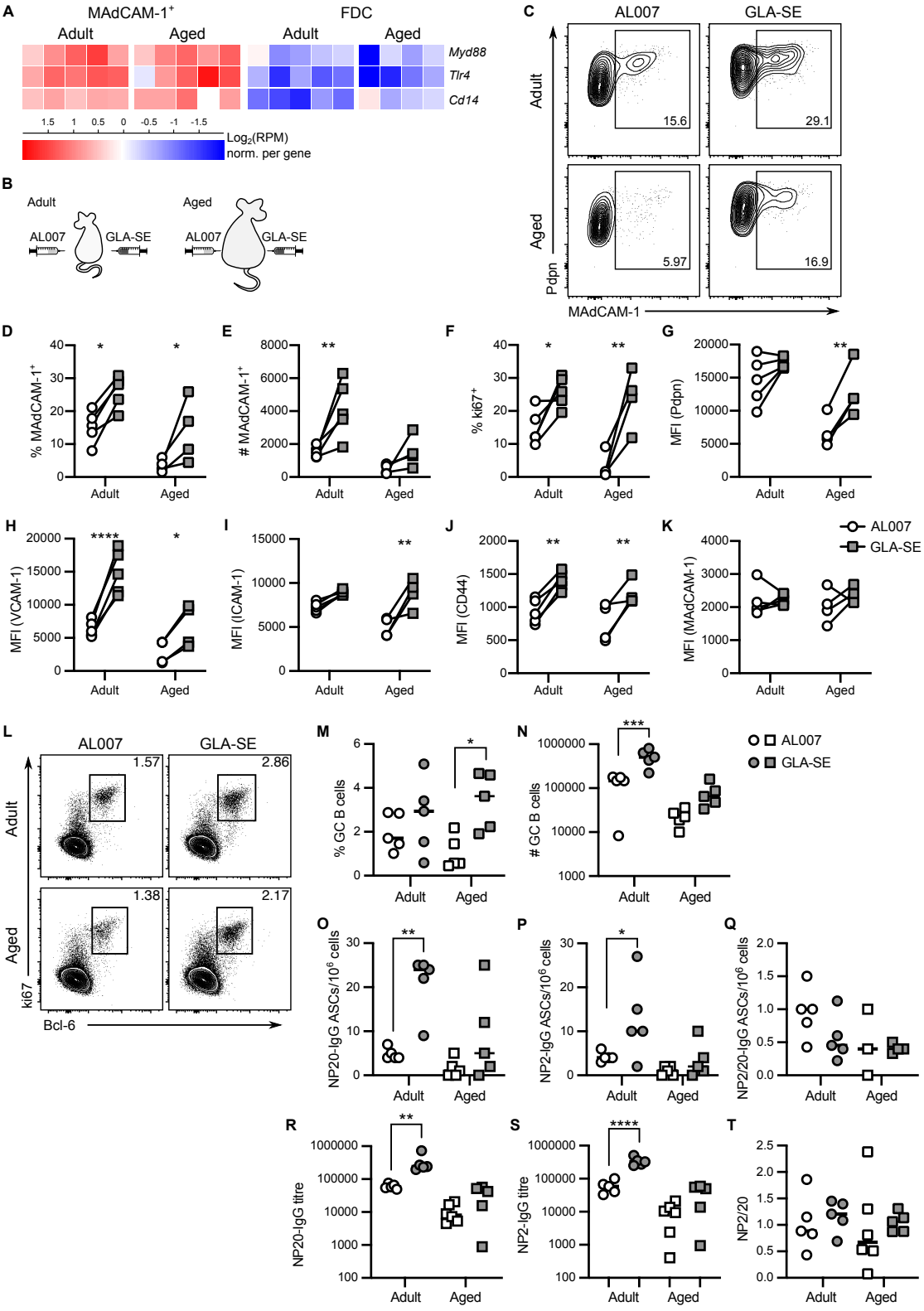

Figure 7. TLR4-adjuvanted vaccination boosts MAdCAM-1⁺ lymphoid stromal cell and GC responses in aging. (A) RNA sequencing data from MAdCAM-1⁺ lymphoid stromal cells and FDCs isolated from naïve y Adult (8-12week old) and aged (>98 week old) C57BL/6 mice were mined for the expression of *Tlr4*, *Cd14* and *Myd88*. Data are represented

as log_2(RPM) counts normalized per gene (n=5). (B-K) Adult (8-12week old) and aged (>98 week old) C57BL/6 mice were administered 50μg NP-KLH in AL007 or GLA-SE on opposing flanks (B) and the MAdCAM-1$^+$ lymphoid stromal cell response determined four days later. MAdCAM-1$^+$ lymphoid stromal cells were measured as the proportion of MAdCAM-1$^+$ cells amongst CD45$^-$CD31$^-$CD21/35$^-$Pdpn$^+$ stromal cells (C, D) and in absolute number (E). The proliferation of MAdCAM-1$^+$ lymphoid stromal cells was measured by ki67 expression (F), and the cell surface expression of Pdpn (G), VCAM-1 (H), ICAM-1 (I), CD44 (J) and MAdCAM-1 (K) were also determined. (L-T) Adult (8-12week old) and aged (>98 week old) C57BL/6 mice were administered 50μg NP-KLH in AL007 or GLA-SE and the GC response and output determined 21d later. Shown are flow cytometry gating (L), the proportion (M) and total number (N) of GC B cells in the dLN, the number of low (O) and high (P) affinity IgG-producing ASCs in the bone marrow, the ratio of high:low affinity ASCs (Q), as well serum antibody levels, showing low (R) and high (S) affinity antibody titres, and the ratio of high:low antibodies (T). Data in (C-T) are representative of at least two independent experiments with 5-7 mice per group. Paired immunizations in individual mice are linked by a line (D-K). Statistical significance was determined using a paired two-way ANOVA (D-K) or a one-way ANOVA (M-T) with Sidâk's multiple comparison test, comparing AL007 to GLA-SE within each age group, * $p<0.05$, ** $p<0.01$, *** $p<0.001$, **** $p<0.0001$.

SUPPLEMENTAL INFORMATION

Supplemental Methods

Mice

C57BL/6, Balb/c, CD45.1^{+} C57BL/6.SJL and *Tlr4*$^{-/-}$ mice were bred and housed in the Babraham Institute Biological Support Unit. *Il33*$^{cit/cit}$ mice were housed in MRC-LMB Ares unit. No primary pathogens or additional agents listed in the FELASA recommendations were detected during health monitoring surveys of the stock holding rooms. Ambient temperature was 19-21^{o}C and relative humidity 52% in the BI-BSU or 45-65% in MRC-LMB Ares unit. Lighting was provided on a 12-hour light: 12-hour dark cycle including 15 min 'dawn' and 'dusk' periods of subdued lighting. After weaning, mice were transferred to individually ventilated cages (GM 500: Techniplast) with up to five mice per cage. Mice were fed CRM (P) VP diet (Special Diet Services, #801722) ad libitum and received seeds (e.g., sunflower, millet) at the time of cage-cleaning as part of their environmental enrichment. All UK mouse experimentation was approved by the Babraham Institute or MRC-LMB Ares Animal Welfare and Ethical Review Body and the UK Home Office. Animal husbandry and experimentation was conducted in accordance with existing European Union and United Kingdom Home Office legislation and local standards. Parabiosis experiments were conducted at the Animal Research Centre, University of Leuven, Belgium using aged C57BL/6 mice purchased from Charles River (UK) and C57BL/6 and CD45.1^{+} mice bred and aged in-house. All Belgian mice were housed under specific pathogen-free conditions and fed ssniff® R/M-H chow (4.7% w/v sugar, 3.3% w/v fat, 19% w/v protein) and were used in accordance the University of Leuven Animal Ethics Committee and existing European Union standards. Adult mice were 8-12 weeks old and aged mice were 90-105 weeks old when used for experiments. For parabiosis experiments, only female mice were used. All other experiments were conducted use sex-matched controls, and both male and female cohorts were used.

Immunizations

Mice were immunized with 50μg of NP-KLH (4-hydroxy-3-nitrophenylacetyl-Keyhole Limpet Hemocyaninin, conjugation ratio 29-33; Biosearch technologies, #N-5060) dissolved in PBS at 2mg/mL and emulsified at a 1:1 ratio with Imject Alum Adjuvant (ThermoFisher Scientific, #77161). For GLA-SE experiments, 50μg of NP-KLH was emulsified in 5μg of GLA-SE or the control adjuvant, Alhydrogel (AL007), (both from IDRI). For LPS experiments, 5μg of LPS (Sigma, #L3102) was added to Imject Alum. Mice received 50μL subcutaneously on each flank at the inguinal LN site under inhalation anesthesia. LNs were harvested after two, four, seven, 14 or 21 days and processed for analysis. Parabionts were immunized on the upper and lower flanks, draining the axillary and brachial LNs as well as the inguinal site. LNs in parabiosis experiments were harvested seven days after immunization. Blood samples were collected by cardiac puncture at the time of dissection to determine blood chimerism for parabiotic pairs.

Parabiosis

Parabiosis was conducted essentially as described (*77-79*). Congenically distinct (CD45.1 and CD45.2) female C57BL/6 mice were cohoused for two weeks prior to surgery to ensure harmonious cohabitation. Surgery was conducted under inhalation anesthesia according to LASA Dhiel guidelines. One incision was made from elbow to knee on corresponding lateral sides and the skin separated from the subcutaneous fascia by blunt dissection. The right olecranon of one mouse was attached to the left olecranon of the second mouse with a single suture; this was repeated for the knee joint. The dorsal and ventral skins were anastomosed by continuous suture. Mice we administered analgesia (10mg/kg Carprofen) intraperitoneally twice daily for 48hr. Parabionts were housed as single pairs with free access to food and water and monitored daily for clinical signs. Mice that appeared in distress (hunching, piloerection) were humanely killed. Three weeks after surgery, mice were immunized as above on the outer flanks. Seven days after immunization, blood and LN samples were collected and analyzed.

Mice that failed to parabiose (<20% of B cells from the partner mouse) were excluded from further analysis.

Cell isolation

For analysis of stromal cells, single cell suspensions were generated by enzymatic digestion as described (*80, 81*). Briefly, LN capsules were pierced with fine forceps and incubated with 0.5mL digestion buffer at 37°C for 20mins and tubes inverted every 5min. After 20mins LNs were triturated with a 1mL pipette tip and supernatant containing released cells was collected to ice-cold buffer comprising PBS containing 2% FCS and 2mM EDTA. Remaining fragments were digested twice more as described, triturating with a 1mL pipette at 5min intervals. Digestion buffer comprised 0.2mg/mL Collagenase P (Sigma, #11213865001), 0.8 mg/mL Dispase II (Sigma #4942078001) and 0.1mg/mL DNase I (Sigma, #10104159001) in RPMI 1640 media (Gibco, #11875093). Cell suspensions were passed through a 70μm mesh prior to staining. For analysis of GC B cells, LNs were forced through a 40μm mesh in PBS containing 2% FCS. In some experiments GC B cells were analyzed from single cell suspensions prepared by enzymatic digestion, as for stromal cell analysis.

Flow cytometry

Cells were stained using cocktails of antibodies. Fc receptors were blocked prior to staining using anti-CD16/32 (93, ThermoFisher, #14-0161). Where >1 brilliant violet or brilliant UV dye was used concurrently, cells were stained using BD brilliant stain buffer (BD Biosciences #563794). Cells were fixed and permeabilized for intracellular/nuclear staining using the eBioscience Foxp3/Transcription Factor Fixation/Permeabilization Staining buffer set (ThermoFisher, #00-5523-00). Samples were stained for 1hr at 4°C (extracellular) or room temperature (intracellular/nuclear) and fixed/permeabilized for 30mins at 4°C. Antibodies used were directed against: CD45 (30-F11, BioLegend), CD31 (MEC13.3, Biolegend or BD Biosciences), Pdpn (8.8.1, BioLegend), MAdCAM-1 (MECA-367, BioLegend), CD21/35

(7E6, BioLegend; eBio8D9, ThermoFisher), ICAM-1 (YN1/1.7.4, BioLegend), VCAM-1 (MVCAM.A, BioLegend), CD44 (IM7, BioLegend), ki67 (SolA15, ThermoFisher), B220 (RA3-6B2, BioLegend), CD4 (GK1.5 or RM4-5, BioLegend or ThermoFisher), Bcl-6 (K112-91, BD Biosciences), TLR4/MD2 Complex (MTS510, ThermoFisher), rat IgG2a isotype control (RTK2758, Biolegend) and CD14 (Sa2-8, ThermoFisher). In some experiments, biotinylated antibodies were detected with BUV395-conjugated streptavidin (BD Biosciences, #564176). Dead cells were excluded with Fixable live/dead e780 (ThermoFisher, #65-0865-18). Samples were acquired on a BD LSRFortessa (BD Biosciences) harboring 355, 405, 488, 561 and 640nm lasers and analyzed using FlowJo software (TreeStar).

Immunofluorescence microscopy

LNs were immersion-fixed in periodate-lysine-paraformaldehyde containing 1% PFA (Sigma, #P6148), 0.075 M L-lysine (Sigma, #L5501), 0.37 M sodium phosphate (pH 7.4, Sigma, #342483), and 0.01 M $NaIO_4$ (Sigma, #210048) for five hours at 4°C, washed, cryoprotected in 30% sucrose (Sigma, #S0389) overnight at 4°C, embedded in optimal cutting temperature medium (VWR, #25608-930) on a dry ice/ethanol bath and stored at -80°C. Sections (15-20µm) were cut at -16°C on a cryostat (Leica), air-dried overnight and stored at -20°C (short-term) or -80°C (long-term). For staining, sections were defrosted and air-dried overnight at room temperature, rehydrated with PBS containing 0.05% Tween-20 (PBST), permeabilized with 2% Triton X-100 (Sigma, #X100) for 15min at room temperature and blocked in PBST containing 1% BSA for 1hr at room temperature. Tissues sections were stained with antibodies: RANKL-biotin (IKK2/5, BioLegend), ki67-FITC (SolA15, ThermoFisher), CD21/35-Alexa Fluor 594 (7E9, BioLegend), CD35-biotin (8C12, BD Biosciences), Lyve-1 (103-PA50AG, ReliaTech), MAdCAM-1-PE (MECA-367, BioLegend) and/or B220-APC (RA3-6B2, BioLegend) overnight at 4°C. Non-conjugated antibodies were detected with Alexa Fluor 647-conjugated streptavidin (S21374, Thermofisher) or Alexa Fluor 488-conjugated goat anti-rabbit IgG (A-11034, Thermofisher), as appropriate, for 2hr at room

temperature. Sections were washed, mounted in aqueous mounting media (HydroMount; National Diagnostics, #HS-106) and allowed to dry prior to imaging. Images of MAdCAM-1 staining were obtained using a Leica DM4B widefield microscope bearing 405-, 488-, 555-, and 640nm lasers alongside DAPI, L5, RHO and Y5 filter cubes using a 10x/0.25 dry objective. Images of ki67 staining were obtained Zeiss LSM880 confocal microscope harboring 405-, 432-, 488-, 561-, and 633-nm lasers using a 40x/1.40 oil objective. Image channels were collected separately and analyzed and compiled using Fiji software (National Institutes of Health).

RNA sequencing and analysis

Stromal cells were released from LNs by enzymatic digestion as described above. Hematopoietic cells were depleted using anti-CD45 microbeads (Miltenyi Biotec, 130-052-301) (7μL/10^7 cells), a QuadroMACS magnet (Miltenyi Biotec) and LS columns (Miltenyi Biotec, 130-042-401), according to manufacturer's instructions. The $CD45^-$ fraction was retained and stained with live-dead e780 and antibodies directed against CD45, Pdpn, CD31, MAdCAM-1 and CD21/35 as described above. MAdCAM-1^+ lymphoid stromal cells (MAdCAM-$1^+CD21/35^-Pdpn^+CD31^-CD45^-$) or FDCs ($CD21/35^+Pdpn^+CD31^-CD45^-$) from unimmunized or immunized adult (8 weeks old) and aged (>95 weeks old) mice were sorted directly into 8.5μL of lysis buffer supplied with the SMART-Seq v4 Ultra low Input RNA kit for Sequencing (Clontech, #634890). Where feasible, we matched the number of sorted MAdCAM-1^+ lymphoid stromal cells and FDCs between adult and aged samples at each time point to limit input cell number variation in the sequencing data. We performed sequencing on five biological replicates for each group; one aged unimmunized FDC samples was excluded from analysis as it failed post-processing QC, leaving four biological replicates in this group.

cDNA from sorted cells was generated using the SMART-Seq v4 Ultra low input RNA kit (Clontech, #634890) according to manufacturer's instructions. Libraries were prepared with 400pg of cDNA per sample using the Illumina Nextera XT kit (#FC-131-1096) following manufacturer's instructions. cDNA and sequencing library quality were determined using Agilent BioAnalyser High Sensitivity DNA chips (#5067-4626), Qubit dsDNA High sensitivity Assay kit (Invitrogen, #Q32854) on a Qubit 4 fluorometer (Invitrogen), and a KAPA library quantification kit (Roche, #7960140001). Samples were sequenced on a HiSeq 2500 (Illumina, v4 chemistry) as 100bp single-end reads. Analysis was performed using the SeqMonk software package (Babraham Institute, https://www.bioinformatics.babraham.ac.uk/projects/seqmonk/, version 1.47.1) after trimming (Trim Galore v0.4.2) and alignment of reads to the reference mouse genome GRCm38 using HISAT2 (*82*). Reads were quantitated over exons and library size was standardized to reads per million, and then read counts were $\log_2$ transformed. Data were analyzed grouped by cell type. Expressed genes were defined as those with a $\log_2$(RPM)>-4 in at least five biological replicates. PCA was conducted performed on the 1000 most variable genes, as indicated in the figure legends. Differentially expressed genes ($p<0.05$ after Bejamimi and Hochberg correction) were identified using Seqmonk's built-in interface to DESeq2 analysis (*83*) of raw counts in pairwise comparisons: MAdCAM-1$^+$ lymphoid stromal cells from unimmunized mice were compared to cells isolated following immunization for both adult and aged mice, and MAdCAM-1$^+$ lymphoid stromal cells isolated from naïve mice or following immunization were compared between adult and aged mice. To test for differential expression of functionally related genes, the Hallmark gene sets (h.all.v7.2) from MSigDB collections (*84*) were used in Seqmonk's built-in Subgroup Statistics analysis (Kolmogorov-Smirnov test, $p<0.05$; average absolute z-score >0.5).

Enzyme-linked immunospot (ELISpot) assay

HTS HA plates were coated with 0.5µg NP20-BSA or 0.25µg NP2-BSA overnight at 4°C. Plates were washed with PBS and blocked with complete media (RPMI /10%FCS/1x penicillin/streptomycin/50µM 2-mercaptoethanol) for 1hr at room temperature. Bone marrow was extracted from femurs of immunized mice and resuspended at $2x10^7$ cell/mL in complete media. $4x10^6$ cells were added to wells and titrated 1:2 across the plate and incubated overnight at 37°C 5%CO_2. The following day cells were removed, wells were washed five times with PBS/0.05% Tween-20 (v/v), three times with PBS and twice with MilliQ. Spots were detected with horseradish peroxidase-conjugated goat anti-mouse IgG (1:8000, Sigma-Aldrich) in PBS/0.1% BSA/0.05% Tween-20 (v/v) for 1-2hr at room temperature. Wells were washed with 3-5 times with PBS/0.05% Tween-20 (v/v) and twice with MilliQ. Spots were developed with 3-amino-9-ethylcarbazole (AEC) chromogen according to manufacturer's instructions (Sigma-Aldrich). Plates were washed with water and dried before reading on an ImmunoSpot (CTL Cellular Technologies LTD).

Enzyme-linked immunosorbent assay (ELISA)

Standardized ELISA was performed to detect NP-specific IgG in mouse serum. MaxiSorp plates (Nunc) were coated with 0.5µg NP20-BSA or 0.125µg NP2-BSA overnight at 4°C, prior to washing in PBS/0.05% Tween-20 (v/v) and blocking with 1% BSA in PBS (ThermoFisher Scientific) for 1hr at room temperature. Known positive serum (pool of serum from mice immunized multiple times with NP-KLH in Alum), experimental sera and negative control sera were titrated 1:3 (in BSA) and incubated for 2hr at room temperature. Following washing, bound antibodies were detected by addition of horseradish peroxidase-conjugated goat anti-mouse IgG (1:8000, Sigma-Aldrich) for 1-2hr at room temperature. Reactions were developed with 3,3',5,5'-tetramethylbenzidine substrate according to manufacturer's instructions (Sigma-Aldrich). ELISA were read using a PHERAstar FS plate reader, and ELISA units were calculated for each sample using the optical density values of the sample and the parameters of the standard curve.

Supplemental Figures

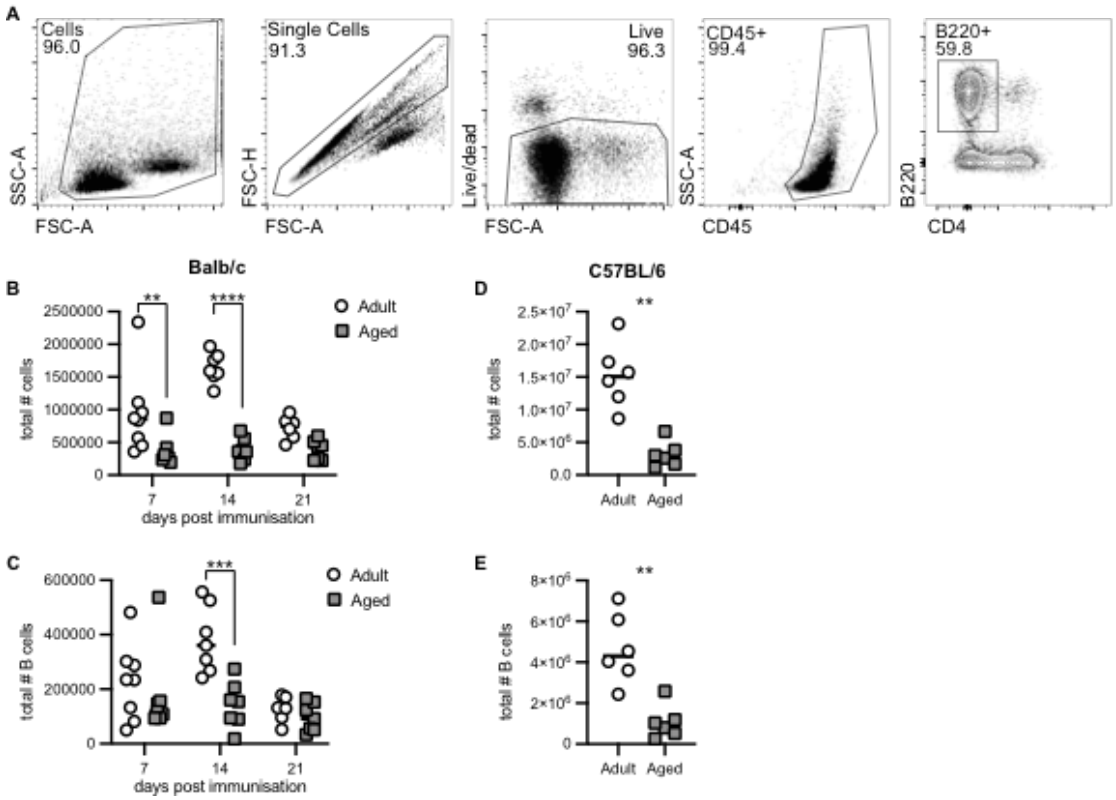

Figure S1. Cellularity in younger adult and aged LNs during immunization. Related to Figure 1. (A) Gating strategy to define B cells. (B-E) Younger adult (8-12week old) and aged (>98 week old) Balb/c (B, C) and C57BL/6 (D, E) mice were immunized as in Figure 1 (A-C) or (D-F). Shown are the total cellularity (B, D) and the number of B cells (C, E). Data are representative of at least two independent experiments with 5-8 mice per group. Statistical significance was determined using a two-way ANOVA with Sidâk's multiple comparison test (B, C) or a Mann-Whitney rank test (D, E). **p<0.01, ***p<0.001, ****p<0.0001.

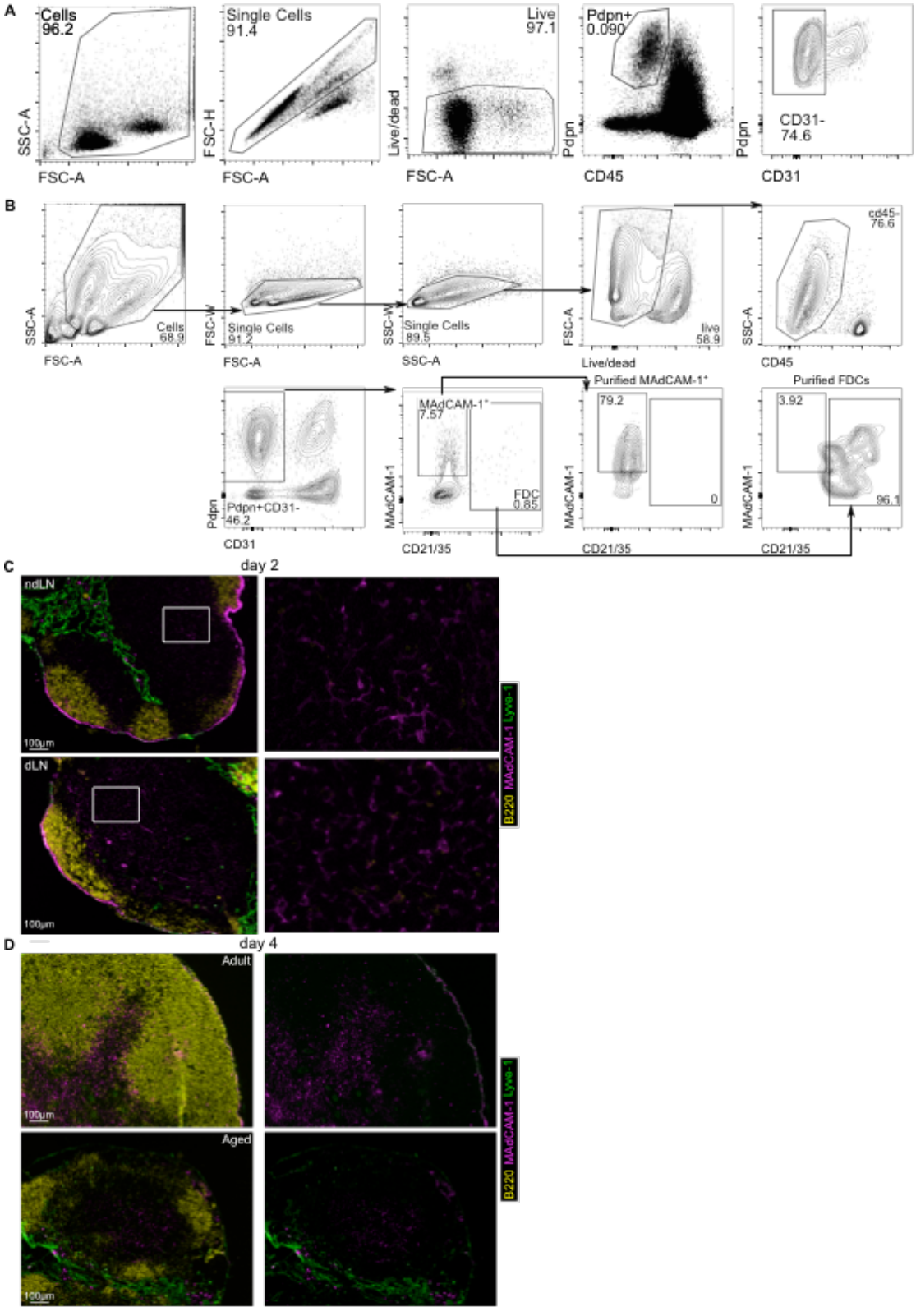

Figure S2. Sort profiles for RNA sequencing and immunofluorescence imaging of MAdCAM-1 expression after immunization. Related to Figure 3. (A) Gating strategy to define lymphoid stromal cells. (B) In order to sort-purify MAdCAM-1$^+$ lymphoid stromal cells and FDCs, cells were first depleted of CD45$^+$ cells using anti-CD45 microbeads and

sorted based on MAdCAM-1 and CD21/35 expression. Cells were gated on FSC and SSC, single cells, live cells, $CD45^-$ cells, $Pdpn^+CD31^-$ cells, then $MAdCAM\text{-}1^+CD21/35^-$ or $CD21/35^+$. Purity of $MAdCAM\text{-}1^+$ lymphoid stromal cells and FDCs was determined by running sorted cells through the cell sorter. $MAdCAM\text{-}1^+$ lymphoid stromal cells were 80% pure and FDCs >95% pure. (C) The expression of MAdCAM-1 by lymphoid stromal cells was determined by immunofluorescence staining on ndLNs and dLNs nodes obtained from younger adult (8-12week old) C57BL/6 mice immunized with 50μg NP-KLH in Alum two days prior. Inset shows MAdCAM-1 expression by T-zone FRCs is present in ndLNs and dLNs. Shown are MAdCAM-1 (magenta), B220 (yellow) and Lyve-1 (green) staining. Scale bar 100μm. (D) The expression of MAdCAM-1 by lymphoid stromal cells was determined by immunofluorescence staining on dLNs obtained from younger adult (8-12week old) and aged (>98 week old) C57BL/6 mice immunized with 50μg NP-KLH emulsified in Alum four days prior. Shown are MAdCAM-1 (magenta), B220 (yellow) and Lyve-1 (green) staining. Scale bar 100μm.

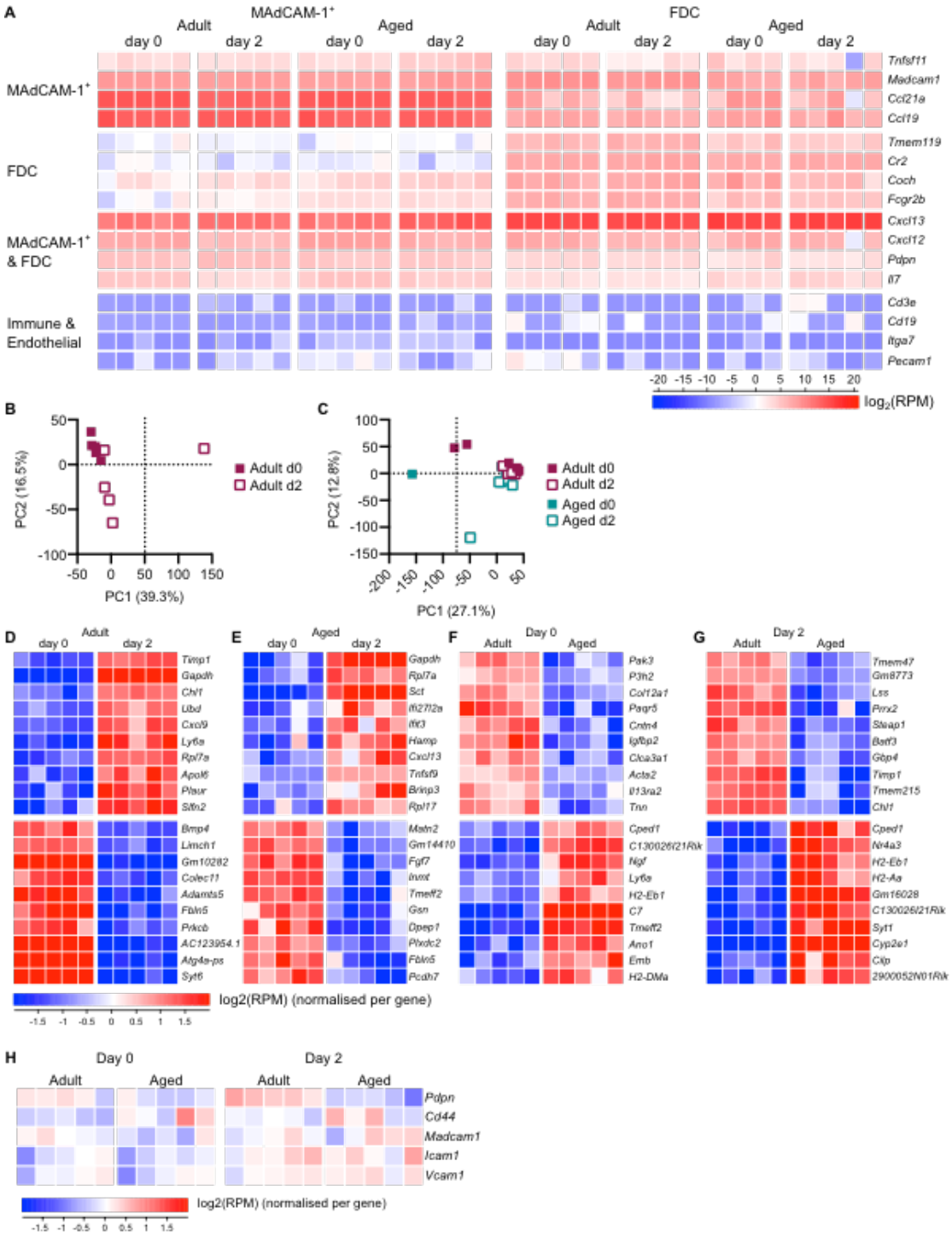

Figure S3. MAdCAM-1⁺ lymphoid stromal cell and FDC identity and differential gene expression, as determined by RNA sequencing. Related to Figure 3. MAdCAM-1⁺ lymphoid stromal cells and FDCs were sort-purified from four groups of C57BL/6 mice: younger adult (8-12week old) and aged (>98 week old) mice, both unimmunized (day 0) and two days after immunization (day 2) with 50µg NP-KLH in Alum and subjected to bulk RNA

sequencing. (A) The expression of genes associated with MAdCAM-1$^+$ lymphoid stromal cells (*Tnfsf11*, *Madcam1, Ccl21a, Ccl19*), FDCs (*Tmem119, Cr2*, *Coch, Fcgr2b*), both MAdCAM-1$^+$ lymphoid stromal cells and FDCs (*Cxcl13, Cxcl12, Pdpn, Il7*), and genes associated with immune cells or endothelial cells (*Cd3e*, *Cd19, Itga7*, *Pecam1*) was determined in all datasets (n=4-5). Data are represented as $\log_2$(RPM) normalized counts, as indicated by the color scale (bottom). (B-C) PCA of FDCs isolated from younger adult mice both before and after immunization (B), and FDCs isolated from younger adult and aged mice, both before and after immunization (C). PCA was performed using the 1000 most variable genes within each analysis. (D-G) The top ten genes, as determined by $\log_2$(foldchange), that were up- and down-regulated in pairwise comparisons of MAdCAM-1$^+$ lymphoid stromal cells RNA sequencing. Pairwise comparisons are between unimmunized and immunized MAdCAM-1$^+$ lymphoid stromal cells isolated from adult (D) and aged (E) mice, and also between adult and aged MAdCAM-1$^+$ lymphoid stromal cells isolated from unimmunized (F) and immunized (G) mice. (H) The mRNA levels for genes found to be upregulated after immunization in younger adult MAdCAM-1$^+$ lymphoid stromal cells by flow cytometry, *Pdpn*, *Cd44*, *Madcam1*, *Icam1* and *Vcam1*, were determined from RNA sequencing data in younger adult and aged MAdCAM-1$^+$ lymphoid stromal cells. Data in (D-H) are represented as $\log_2$(RPM) counts normalized within each gene, as indicated by the color scale (bottom), where each square represents a biological replicate (n=5).

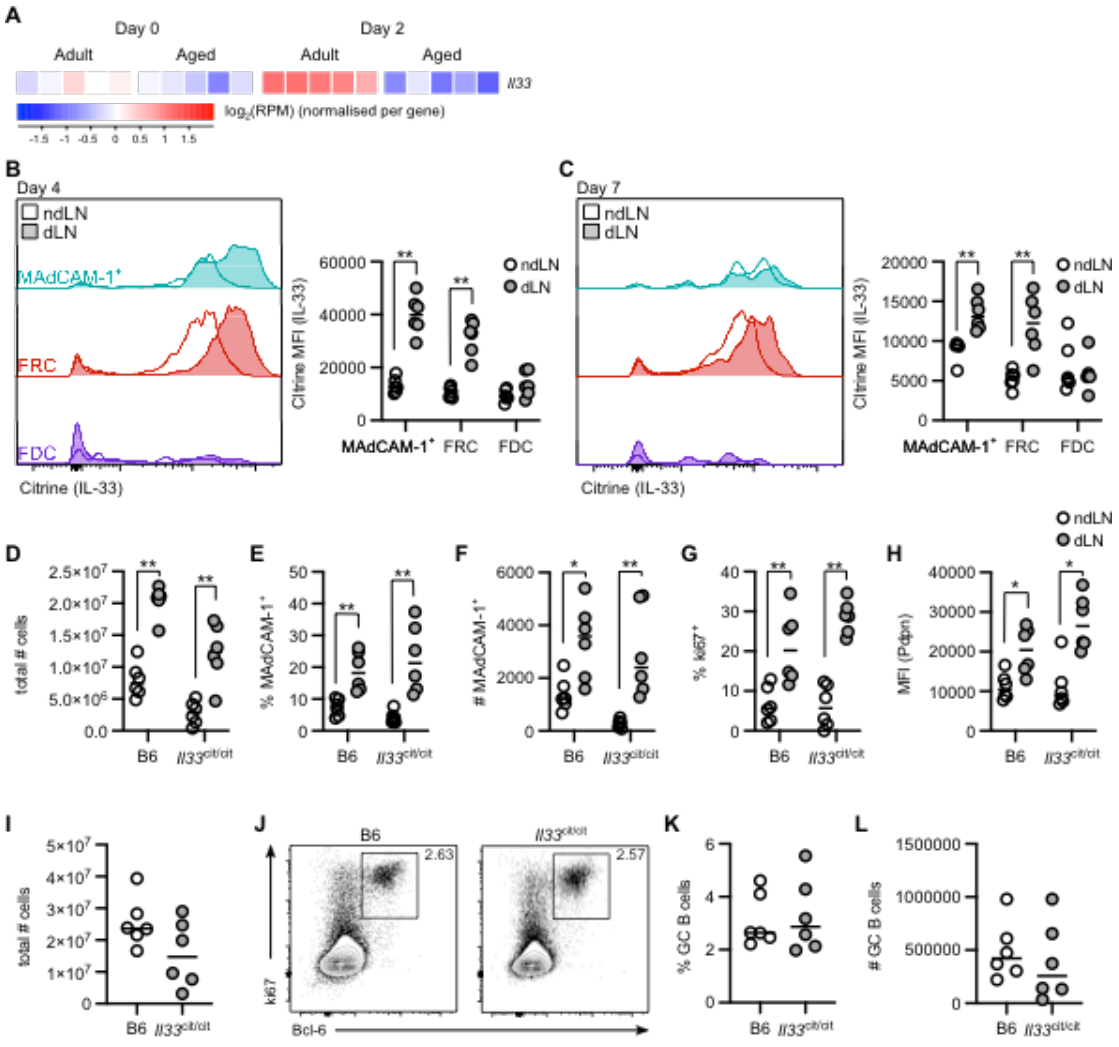

Figure S4. IL-33 expression by MAdCAM-1⁺ lymphoid stromal cells is increased after Alum-adjuvanted immunization, but does not affect the GC response. Related to Figures 3 and 4. (A) *Il33* expression was determined in younger adult (8-12week old) and aged (>98 week old) MAdCAM-1⁺ lymphoid stromal cells from RNA sequencing data. Data in (D-H) are represented as $\log_2$(RPM) counts normalized within each gene, as indicated by the color scale (bottom), where each square represents a biological replicate (n=5). (B-C) IL-33 expression by lymphoid stromal cells was determined by the MFI of Citrine expression in *Il33*$^{cit/cit}$ mice (8-12 week old) both four (B) and seven (C) days after immunisation with NP-KLH+Alum. Shown are histograms of Citrine expression in MAdCAM-1⁺ lymphoid stromal cells, MAdCAM-1-negative FRCs and FDCs from ndLNs (empty histograms) and dLNs (filled histograms), alongside graphed data. (D-H) The impact of lack of IL-33 expression on

the MAdCAM-1$^+$ lymphoid stromal cell response was determined four days after immunization in *Il33*$^{cit/cit}$ (knockout) mice and C57BL/6 controls. Shown are the total LN cellularity (D), the proportion (E) and absolute number (F) of MAdCAM-1$^+$ lymphoid stromal cells, as well as the proportion of proliferating MAdCAM-1$^+$ lymphoid stromal cells (G) and the MFI of Pdpn (H) in ndLNs and dLNs. (I-L) The impact of lack of IL-33 expression on the GC response was determined seven days after immunization in *Il33*$^{cit/cit}$ (knockout) mice and C57BL/6 controls. Shown are the total LN cellularity (I), gating for GC B cells (J) as well as the proportion (K) and absolute number (L) of GC B cells in the dLN. Data are representative of one experiment per timepoint (n=6). Statistical significance in (B-H) was determined with multiple Mann-Whitney tests comparing ndLNs and dLNs within each genotype, *$p<0.05$, ** $p<0.01$. Statistical significance in (I-L) was determined with Mann-Whitney rank test between mouse strains (all non-significant).

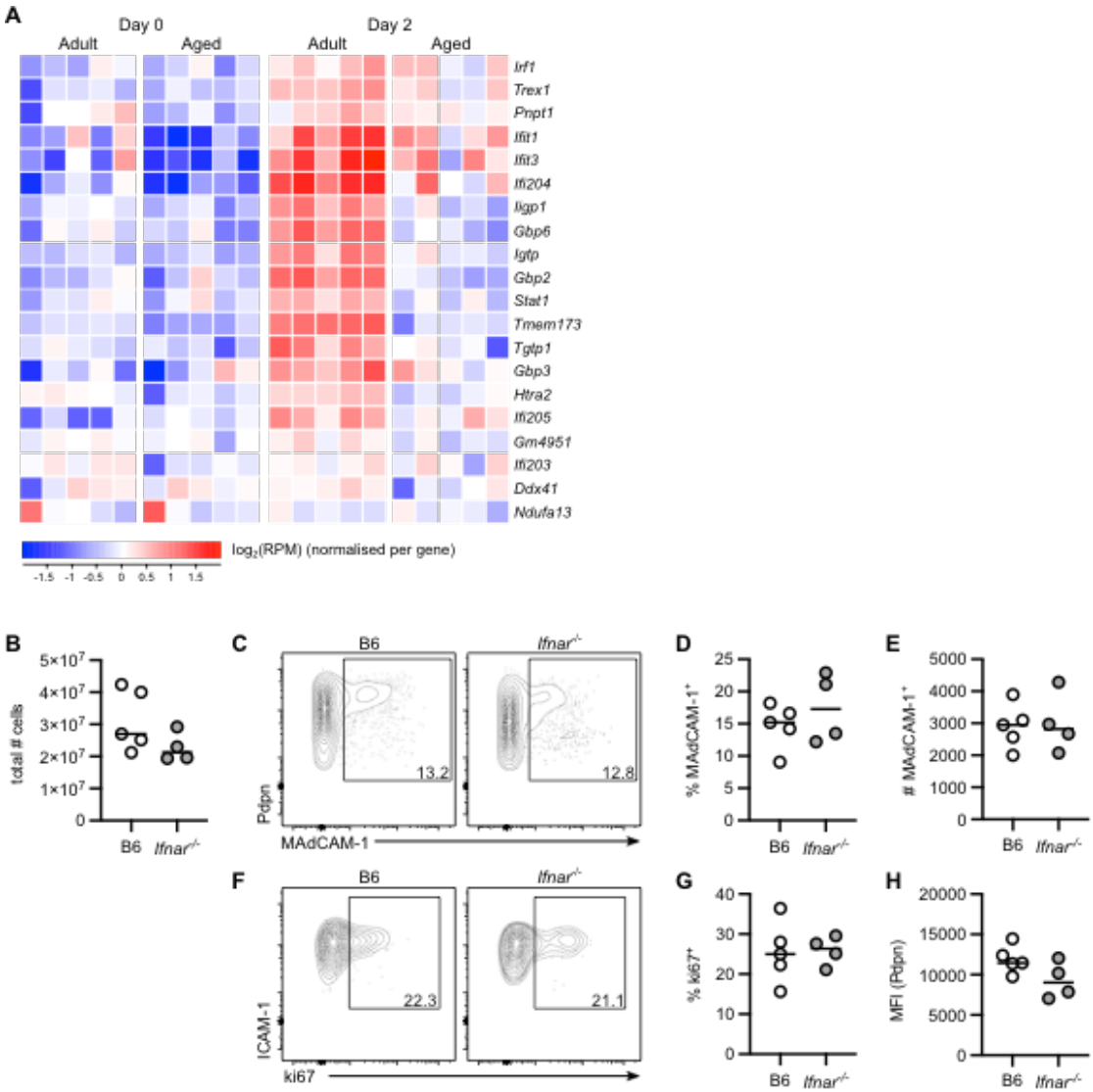

Figure S5. Lack of type I IFN signaling does not impact the MAdCAM-1⁺ lymphoid stromal cell response to immunization. Related to Figure 4. (A) The mRNA levels of type I IFN response genes were determined in MAdCAM-1⁺ lymphoid stromal cells isolated from younger adult (8-12week old) and aged (>98 week old) C57BL/6 mice before and 2d after immunization with NP-KLH+Alum by RNAseq. (B-H) Adult (8-12 week old) *Ifnar*$^{-/-}$ and C57BL/6 control mice were administered NP-KLH+Alum and the MAdCAM-1⁺ lymphoid stromal cell response was determined four days later. Shown are the total LN cellularity (B), gating for MAdCAM-1⁺ lymphoid stromal cells (C), and graphical data showing the proportion (D) and absolute number (E) of MAdCAM-1⁺ lymphoid stromal cells. MAdCAM-1⁺ lymphoid stromal cell responsiveness was measured by proliferation (F, G) and upregulation of Pdpn (H). Data in (B-H) are representative of two independent experiments

(n=4-6) and statistical significance was determined using a Mann-Whitney rank test (all non-significant).

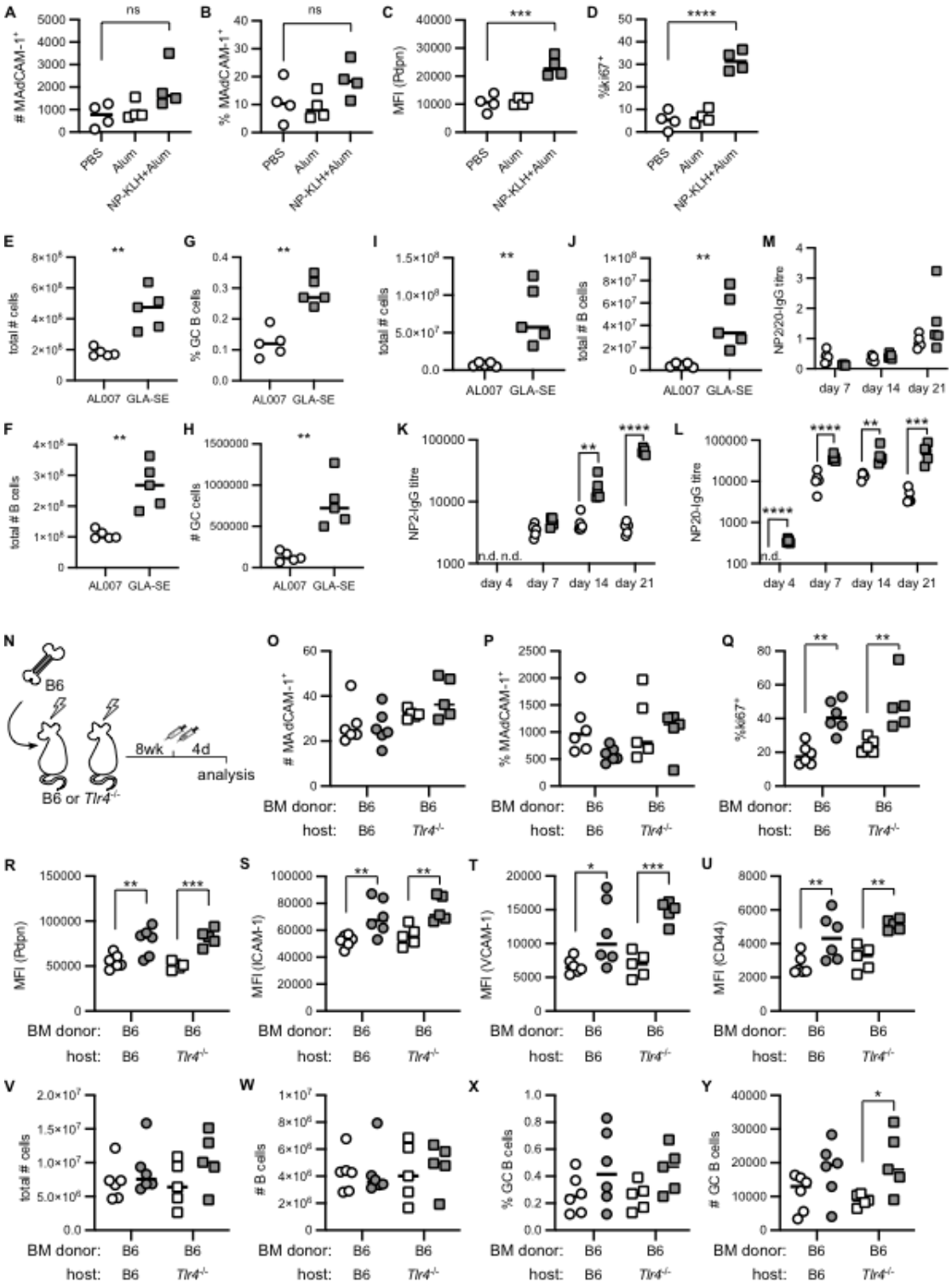

Figure S6. Targeting TLR4 boosts the MAdCAM-1⁺ lymphoid stromal cell and GC response to immunization, and TLR4 expression by immune cells promotes MAdCAM-1⁺ lymphoid stromal cell activation. Related to Figure 6. (A-D) Adult (8-12 week old) C57BL/6 mice were administered PBS, Alum or 50μg NP-KLH in Alum subcutaneously and

the MAdCAM-1$^+$ lymphoid stromal cell response was determined four days later. The MAdCAM-1$^+$ lymphoid stromal cell response was measured as the absolute number (A) and proportion of MAdCAM-1$^+$ cells within the CD45$^-$CD31$^-$CD21/35$^-$Pdpn$^+$ population (B), the MFI of Pdpn (C) and the proportion of proliferating cells (D). (E-H) Adult (8-12 week old) C57BL/6 mice were administered 50μg NP-KLH in AL007 or GLA-SE on opposing flanks and the GC response was determined four days later. Shown are the total LN cellularity (E), the absolute number of B cells (F) and the proportion (G) and absolute number (H) of GC B cells. (I-M) Adult (8-12 week old) C57BL/6 mice were administered 50μg NP-KLH in AL007 or GLA-SE and the GC response and output was determined 21 days later. Shown are the total LN cellularity (I), the absolute number of B cells (J) and serum antibody titres, measuring high (K) and low (L) affinity antibodies and the ratio of high:low affinity antibodies (M) over a timecourse. (N-Y) CD45.1$^+$ C57BL/6.SJL bone marrow donors were used to reconstitute irradiated C57BL/6 and *Tlr4*$^{-/-}$ hosts to generate chimeric animals in which TLR4 expression is absent on radioresistant cells but present on hematopoietic cells. Eight weeks after reconstitution, mice were administered 50μg NP-KLH emulsified in AL007 or GLA-SE on opposing flanks and the MAdCAM-1$^+$ lymphoid stromal cell and GC responses were determined four days later (N). MAdCAM-1$^+$ lymphoid stromal cell responses were measured by proportion (O) and in absolute number (P). MAdCAM-1$^+$ lymphoid stromal cell proliferation was measured by ki67 staining (Q) and their phenotype was determined by upregulation of Pdpn (R), ICAM-1 (S), VCAM-1 (T) and CD44 (U). The GC response was measured by the total LN cellularity (V), the total number of B cells (W) and the proportion (X) and absolute number (Y) of GC B cells. Data in (A-D) are representative of two independent experiments (n=4 per group) and statistical significance was determined using a one-way ANOVA using Dunnett's multiple comparison test, with Alum and Alum+LPS groups compared to PBS. Data in (E-L) are representative of two independent experiments (n-4-5) and statistical significance was determined using a Mann-Whitney rank test (E-J) or t-tests at each timepoint (K-M), comparing AL007 to GLA-SE. Data in (N-Y) are

representative of two independent experiments (n=6-7) with statistical significance determined using a one-way ANOVA with Sidâk's multiple comparison test, comparing AL007 to GLA-SE within each chimera group, *p<0.05, **p<0.01, ***p<0.001, ****p<0.0001.

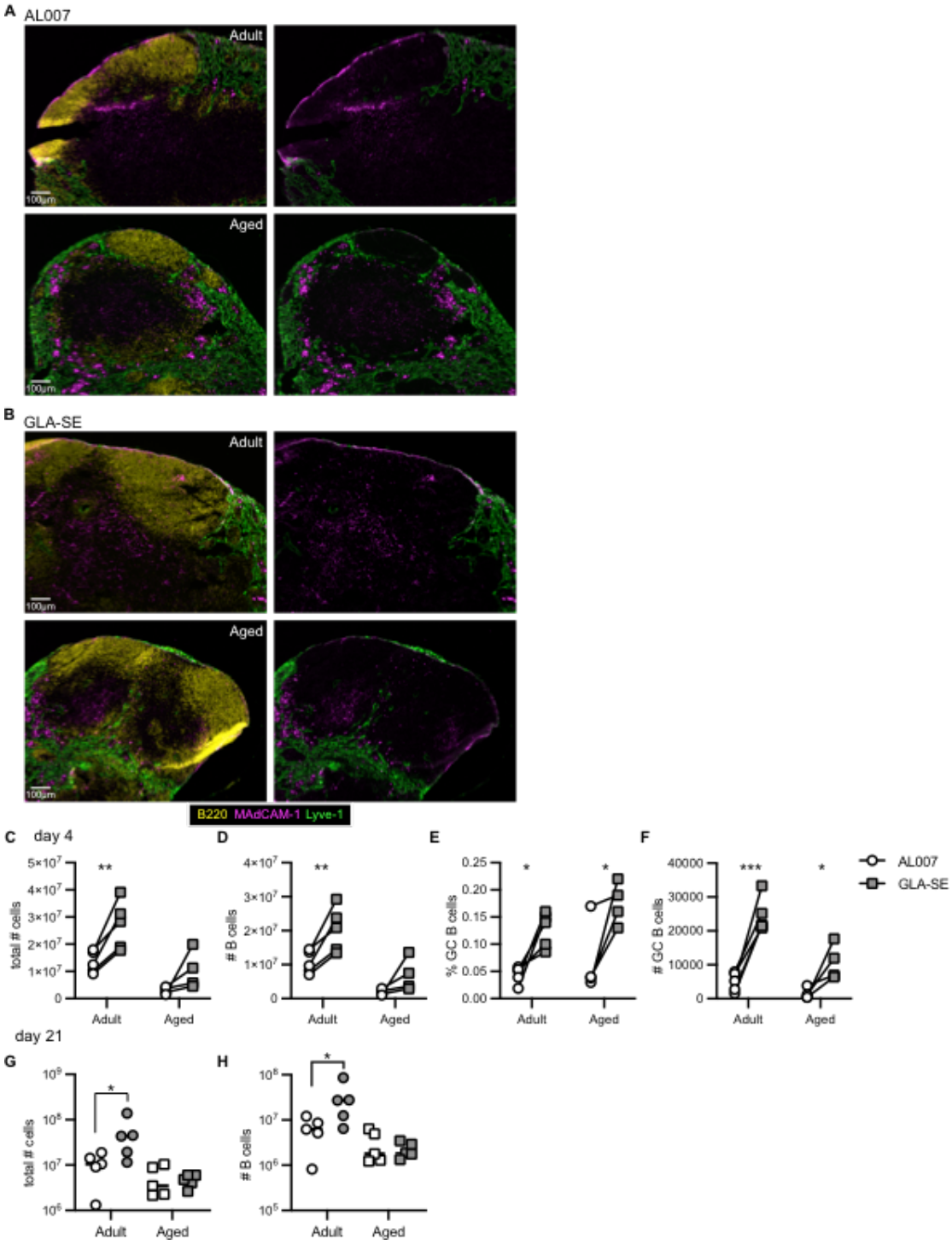

Figure S7. TLR4-adjuvanted vaccination boosts the MAdCAM-1$^+$ lymphoid stromal cell and GC response in aging. Related to Figure 7. (A-B) LN sections from younger adult (8-12week old) and aged (>98 week old) C57BL/6 mice administered 50μg NP-KLH in AL007 (A) or GLA-SE (B) four days prior were stained for B220 (yellow), Lyve-1 (green) and MAdCAM-1 (magenta) by immunofluorescence Scale bars 100μm. (C-F) Younger adult (8-

12week old) and aged (>98 week old) C57BL/6 mice were administered 50μg NP-KLH in AL007 or GLA-SE on opposing flanks and the GC response determined four days later. Shown are the total LN cellularity (C), the absolute number of B cells (D) and the proportion (E) and absolute number (F) of GC B cells. (G-H) Younger adult (8-12week old) and aged (>98 week old) C57BL/6 mice were administered 50μg NP-KLH in AL007 or GLA-SE and the total LN cellularity (G) and absolute number of B cells (H) were determined 21 days later. Data are representative of at least two independent experiments with 5-7 mice per group. Paired immunizations in individual mice are linked by a line (C-F). Statistical significance was determined using a paired two-way ANOVA (C-F) or a one-way ANOVA (G, H) with Sidâk's multiple comparison test, comparing AL007 to GLA-SE within each age group, * $p<0.05$, ** $p<0.01$, *** $p<0.001$.